confirm the diagnosis of LBD.[16] However, the biopsy of olfactory bulb is too invasive and difficult to carry out for patients without risk.[17,18]

The olfactory epithelium is composed of paraneurons and neurites from which the glomeruli of the olfactory bulb originate. However, a neuropathologic analysis of LBAS has not been carried out adequately for LBD. Duda *et al.* reported that normal α-synuclein is expressed in the basal cells, olfactory receptor neurons, supporting cells, and Bowman's glands of the olfactory epithelium in normal controls, as well as patients with Parkinson's disease, Alzheimer disease and multiple system atrophy.[19] However, pathologic α-synuclein accumulation is rare (3.7%) among both normal controls and individuals affected by DLB, Alzheimer disease or Parkinson's disease.[20] According to a biopsy study of the olfactory epithelium in individuals with Parkinson's disease and younger hyposmic controls, no specific pathologic alteration was found.[21]

Therefore, it is still controversial whether abnormal α-synuclein accumulation in the olfactory epithelium precedes the formation of LBs/LNs in the olfactory bulb and contributes to olfactory dysfunction in sporadic Parkinson's disease. The aim of this study was to clarify the neuropathologic alterations of the olfactory mucosa in LBD by immunohistochemical analysis of a series of autopsied individuals.

MATERIALS AND METHODS

Tissue source

Tissue samples were obtained from autopsy materials that were collected at the Tokyo Metropolitan Geriatric Hospital and Institute of Gerontology between October 2008 and August 2010. This hospital is located at the center of Tokyo city and is a geriatric general emergency hospital with 579 beds. This hospital provides community-based medical service to the aged population 24 h/day in cooperation with local general practitioners. The number of autopsy cases was 162 in the above duration. In addition to the general organs, we could obtain the brains and spinal cords from 105 cases in that period, that were registered to the Brain Bank for Aging Research (BBAR) with the deceased's relatives' informed consent. The BBAR is approved by the ethics committee of the Tokyo Metropolitan Geriatric Hospital and Institute of Gerontology to carry out comprehensive research.

Clinical information

All clinical information, including the presence or absence of Parkinsonism as well as dementia, was retrospectively obtained from medical charts and reviewed by two board-certified neurologists.[11,22–26] First, we evaluated Parkinsonism such as bradykinesia, resting tremor, rigidity and postural instability. In this study, when individuals had two or more of these four clinical symptoms, we defined them as having Parkinson's disease-related symptoms.[27] Second, we analyzed scores for the Mini-Mental State Examination[28] or the Hasegawa Dementia Scale (or its revised version),[29,30] the Instrumental Activities of Daily Living,[31] and the Clinical Dementia Rating (CDR).[32] When individuals were not assigned to a category of CDR, we retrospectively determined CDR using medical records, including the battery of cognitive tests above, as well as interviews with attending physicians and caregivers when necessary. Based on these results, we assigned a clinical diagnosis to each patient. The clinical diagnosis of Alzheimer disease was carried out based on the criteria of the National Institute of Neurological and Communication Disorders and Stroke-Alzheimer Disease and Related Disorders Association.[33] The diagnosis of DLB and Parkinson's disease with dementia conformed to the third report of the DLB consortium.[34]

Histology

We examined the brain and olfactory epithelium, olfactory bulb, esophagogastric mucosal junction, sympathetic ganglia, thoracic spinal cord, adrenal glands, anterior wall of the left ventricle of the heart, and abdominal skin.[22,26] The brains and spinal cords were examined as previously reported.[22,24,25] Briefly, the cerebral and cerebellar hemispheres as well as brainstem were dissected in the sagittal plane at the time of autopsy. In each case, half of the brain was preserved at −80°C for further biochemical and molecular analyses. The other half of the brain and abdominal skin were fixed in 20% buffered formalin (WAKO, Osaka, Japan) for 7–13 days and sliced in the same manner as the contralateral hemisphere. The adrenal gland and anterior wall of the left ventricle of the heart were fixed in 20% formalin. The representative areas were embedded in paraffin. Six-micrometer-thick serial sections were cut and stained with HE and KB. Sections of the amygdala, hippocampus, parahippocampal gyrus and temporal cortex were stained with the modified Gallyas-Braak method for senile plaques, NFTs and argyrophilic grains.[35]

Immunohistochemistry

Sections were immunostained using the following antibodies raised against phosphorylated tau protein (p-tau) (AT8, monoclonal; Innogenetics, Temse, Belgium): synthetic peptide corresponding to amino acids 11–28 of amyloid-beta protein (12B2, monoclonal; IBL, Maebashi, Japan); phosphorylated α-synuclein (pSyn#64, monoclonal[25] and

Table 1 Antibodies used for immunohistochemistry

Antibody	Epitope	Source	Clone	Dilution ratio	Antigen method	Retrieval (min)
pSyn#64	α-synuclein phosphorylated ser 129	T. Iwatsubo	Monoclonal	1:20000	99% formic acid	5
PSer129	α-synuclein phosphorylated ser 129	T. Iwatsubo	Polyclonal	1:100	None	
PGP9.5	PGP9.5	Biomol	Polyclonal	1:5000	microwave	30
SMI31	phosphorylated neurofilament	Sternberger	Monoclonal	1:20000	None	
Tyrosine hydroxylase	Anti-tyrosine hydroxylase, rat	CALBIOCHEM	Monoclonal	1:10	microwave	30
AT8	Phosphorylated tau protein	Innogenetics	Monoclonal	1:1000	None	
12B2	Aβ11–28	IBL	Monoclonal	1:50	99% formic acid	5

PSer129 polyclonal[36]), ubiquitin (polyclonal, Sigma-Aldrich, St. Louis, MO), Protein Gene Product 9.5 (PGP9.5, polyclonal; ENZO Life Sciences International, Farmingdale, NY USA); phosphorylated neurofilament (SMI31, monoclonal; Sternberger Immunochemicals, Bethesda, MA, USA); and tyrosine hydroxylase (Anti-Tyrosine Hydroxylase, Rat, monoclonal; Calbiochem-Novabiochem Corporation, Darmstadt, Germany) (Table 1). The signals from monoclonal and polyclonal antibodies were detected by using the automatic system on a VENTANA NX20 with the I-View DAB Universal Kit (Roche, Basel, Switzerland) according to the manufacturer's instructions. Sections were counter-stained with hematoxylin.

LBAS

CNS

In order to analyze LBAS,[22] we carried out immunohistochemical analysis with phosphorylated α-synuclein antibodies for the following sections: the medulla oblongata at the level of the dorsal motor nucleus of the vagus, the upper pons at the level of the locus coeruleus, and the midbrain including the substantia nigra, amygdala, anterior hippocampus and the peripheral nervous system from all cases (described in the next section). When immunopositive deposits were observed in these anatomic regions, we carried out additional immunohistochemical analysis for sections of the basal nucleus of Meynert, anterior cingulate gyrus, entorhinal cortex, the second frontal and temporal gyri and the supramarginal gyrus, using antibodies raised against phosphorylated α-synuclein.

Peripheral nervous system

To analyze LBAS of the peripheral nerve, tissue sections from epicardium and epicardial fat of the left ventricle of the heart, sympathetic ganglia, esophagogastric mucosal junction, adrenal gland[22] and abdominal skin[26] were examined by using antibodies raised against phosphorylated α-synuclein.

Olfactory mucosa

At the time of autopsy, the olfactory mucosa, bony septae and contiguous cribriform plate were removed en bloc (Fig. 1). The cribriform plate was dissected in the sagittal plane of the midline by using an electric jigsaw. The left side was fixed for 24 h in 4% paraformaldehyde. After fixation, the olfactory mucosa was removed, dehydrated in a graded alcohol series, cleared in xylene and embedded in paraffin. The right side was fixed for 24 h in 4% paraformaldehyde, decalcified with EDTA for 2 weeks, and dehydrated and embedded in paraffin. Serial 6-μm-thick sections were stained with HE and immunolabeled with antibodies against phosphorylated α-synuclein, PGP9.5, phosphorylated neurofilament, tyrosine hydroxylase, phosphorylated tau and amyloid β (Table 1). In particular, the olfactory receptor neurons of the olfactory epithelium were identified by using PGP9.5 immunohistochemistry.[19] The normal anatomical appearance of the olfactory system is shown in Figure 2.

Olfactory bulb

The olfactory bulbs were prepared for histologic sections to analyze the presence of LBAS. By using HE stain and α-synuclein antibodies, LBAS were identified in the glomeruli, mitral cells, tufted cells and granular cells as previously reported.[11] Mitral and tufted cells were distinguished by their specific shapes. Each neuron was identified when it had an apparent nucleus containing a prominent nucleolus and Nissl substance.

Semiquantitative scoring system of Lewy-related pathology

For each section, we semi-quantitatively graded the immunohistochemical staining with antibody raised against phosphorylated α-synuclein. Our grading system was modified based on the scoring system of the third report of the DLB consortium[34] because we used both the HE stain and immunohistochemistry using monoclonal antibody for phosphorylated α-synuclein to identify LBAS.

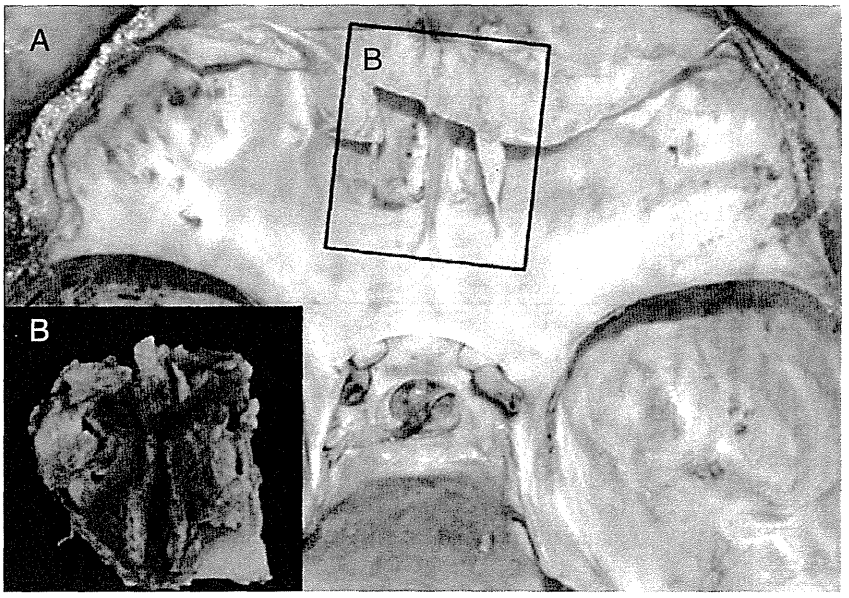

Fig. 1 (a) The anterior cranial fossa after removal of the brain. In order to obtain the olfactory mucosa, the bony septae and contiguous cribriform plate (the rectangular area) were dissected using an electric jigsaw. (b) An inset shows the olfactory mucosa and cribriform plate from the opposite side of the rectangular area.

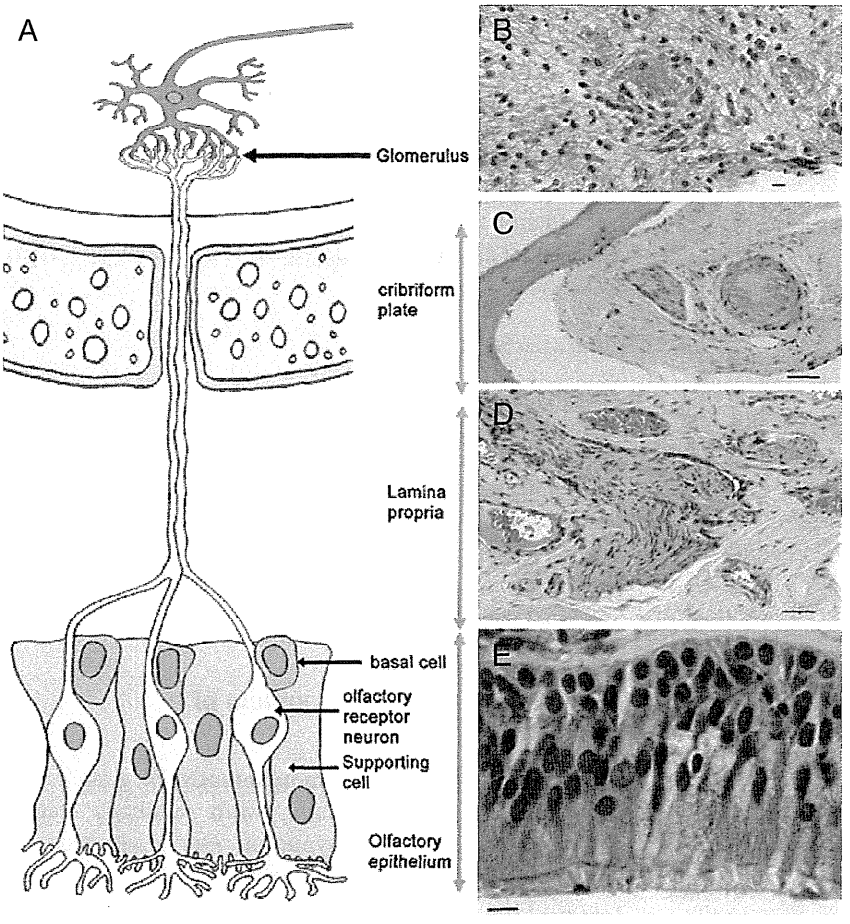

Fig. 2 Scheme of the normal olfactory pathway (a) and photomicrographs of representative histologies of each region (b–e). The olfactory epithelium is composed of three cell types: the basal cells, olfactory receptor neurons and supporting cells (a). The basal cells are the progenitor of the olfactory receptor neurons (a, e). In general, the turnover rate of the olfactory receptor neurons is approximately 30–90 days. Nerve fibers are present in the lamina propria and cribriform plate (c and d, respectively). They consist of either the axons of the olfactory receptor neurons or postganglionic sympathetic nerve fibers. There are glomeruli in the olfactory bulb (b). Glomeruli are the synaptically connected structures of the axons of the olfactory receptor neurons and mitral/tufted cells in the olfactory bulb. (b, e), scale bar = 10 μm; (c), scale bar = 50 μm; (d), scale bar = 100 μm.

For example, 'Stage 1' of the original scoring system was defined as 'sparse Lewy bodies or neurites.' On the other hand, 'Grade 1'of our methodology is defined as 'sparse Lewy neurites without Lewy bodies.'

Grade 0 = neither LNs nor LBs detected using anti-phosphorylated α-synuclein antibody.

Grade 1 = sparse phosphorylated α-synuclein immunopositive dots or neurites, or diffuse granular cytoplasmic stain in the neuron, neither LBs nor phosphorylated α-synuclein-immunopositive neuronal intracytoplasmic dense aggregations.

Grade 2 = 1–3 LBs or phosphorylated α-synuclein-immunopositive intracytoplasmic dense aggregations and scattered LNs in a low-power field (×10).

Grade 3 = more than four LBs and scattered LNs in a low-power field (×10).

Grade 4 = numerous LBs and neurites with severe immunoreactivity for phosphorylated α-synuclein in the neuropil or background.

LB staging system of our BBAR (BBAR LB stage)

In order to assess the clinical and neuropathologic alterations of LBD, we applied the following rating system to our BBAR for all autopsy cases (Table 2, Fig. 3). The original BBAR LB staging system was developed in order to track the individual data of our brain bank.[24,25] This rating system requires clinical symptoms, gross and microscopic neuropathologic alterations, and LB scores used in the consensus guidelines for the clinical and pathologic diagnosis of DLB.[27] In this staging system, Parkinson's disease with

Table 2 Lewey body stage of Brain Bank for Aging Research

Stage	Psyn-IR	LB	SN: loss of pigmentation	LB score	Dementia	Parkinsonism	Diagnosis
0	–	–	–				
0.5	+	–	–				
1	+	+	–				Incidental LBD
2	+	+	+	0–10	–†	–†	Subclinical LBD
3	+	+	+	0–10	–	+	PD
4	+	+	+	3–6	+	+	PDDL
	+	+	+	3–6	+	+ or –	DLBL‡
5	+	+	+	7–10	+	+	PDDN
	+	+	+	7–10	+	+ or –	DLBN‡

†Neither dementia nor Parkinsonism associated with Lewy body-related α-synucleinopathy. ‡Differential diagnosis of PDD and DLB was based on the '1-year rule' according to the consensus guidelines (34). DLBL, dementia with Lewy bodies and a Lewy body score corresponding to the limbic form; DLBN, dementia with Lewy bodies and a Lewy body score corresponding to the neocortical form; LB, Lewy body; LBD, Lewy body disease; PD, Parkinson's disease; PDDL, Parkinson's disease with dementia and a Lewy body score corresponding to the limbic form; PDDN, Parkinson's disease with dementia and a Lewy body score corresponding to the neocortical form; Psyn-IR, phosphorylated alpha-synuclein immunoreactivity; SN, substantia nigra.

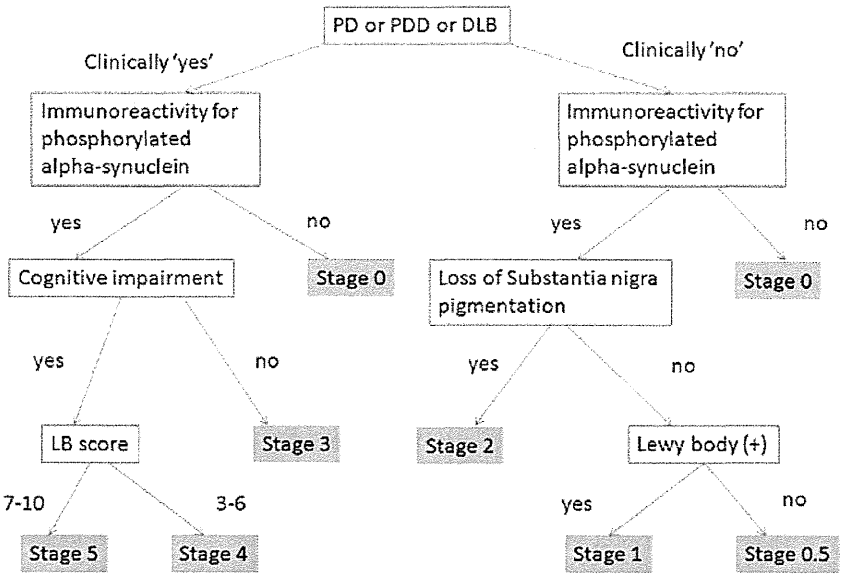

Fig. 3 Flow-chart of the Lewy body staging system of the Brain Bank for Aging Research (BBAR). PD, Parkinson's disease; PDD, Parkinson's disease with dementia; DLB, dementia with Lewy bodies; SN, substantia nigra; LB score, Lewy body score. See Table 2 for detailed description of each stage.

dementia was differentiated from DLB by applying the '12-month (1-year)' rule noted in the Consensus Guidelines (i.e., 'dementia appears more than one year after the onset of Parkinsonism').[27]

Evaluation of senile changes and neuropathologic diagnosis

NFTs were classified according to Braak and Braak's staging system using modified Gallyas-Braak staining[37] and AT8 immunohistochemistry.[38] The staging system for senile plaques (SPs) comprises four stages (0–C). Argyrophilic grains were classified into our four stages (0–III), as reported previously.[23] The neuropathologic diagnosis of Alzheimer disease was based on our previous definition,[39] which proposed a modification of the National Institute on Aging and Reagan Institute criteria.[40,41] The diagnoses of dementia with grains and NFT-predominant forms of dementia were based on the previously described definitions.[42,43]

Statistical analysis

Fisher's exact test was carried out to compare the number of cases having LBAS pathology in the olfactory mucosa.

RESULTS

Clinical information

Of the 105 consecutive autopsy patients, 58 were men and 47 were women. The patient ages at death ranged from 65 to 104 years (82 ± 37, mean ± SD). Twelve patients showed Parkinson's disease-related symptoms according to the clinical criteria in this study. Six out of 105 patients were clinically diagnosed as LBD including Parkinson's disease, Parkinson's disease with dementia and DLB.

Neuropathologic diagnosis

The neuropathologic diagnoses consisted of Alzheimer disease ($n = 15$), dementia with grains ($n = 11$), NFT-predominant form of dementia ($n = 8$), Parkinson's disease ($n = 2$), Parkinson's disease with dementia ($n = 2$), and DLB ($n = 1$), as well as one case each of dentatorubral-pallidoluysian atrophy, neuronal hyaline inclusion body disease, frontotemporal lobar degeneration with transaction response (TAR) DNA-binding protein-43 kDa-immunoreactive inclusions, and progressive multifocal leukoencephalopathy. Patients with combined pathologies, included Alzheimer's disease plus DLB ($n = 2$), dementia with grains plus NFT-predominant form of dementia ($n = 3$), and one patient each of diffuse NFTs with calcification (DNTC)[44] plus DLB and dementia with grains plus Alzheimer's disease. The remaining patients did not fulfil the clinical and/or pathological criteria for neurodegenerative diseases.

Eight out of 105 patients (8/105 = 7.6%) were clinically and neuropathologically diagnosed as having LBD, including Parkinson's disease (2 patients), Parkinson's disease with dementia (2 patients) and DLB (4 patients).

Incidence, distribution and extent of LBAS

BBAR staging

Based on clinical and neuropathologic analyses, the BBAR LB stages were as follows: stage 0 = 66 cases, stage 0.5 = 6 cases, stage 1 = 21 cases, stage 2 = 4 cases, stage 3 = 2 cases, stage 4 = 3 cases and stage 5 = 3 cases. All of the stage 5 cases had DLB, with an LB score corresponding to the value for the neocortical form (DLBN).

LBAS in CNS and peripheral nervous system

We identified 39 (37.1%) out of the 105 individuals with α-synuclein immunopositive LBAS in the CNS or peripheral nervous system (Table 3). Therefore, we focused on these 39 cases in the present study. Here, LBAS was identified by using α-synuclein immunohistochemistry. In LBAS, LBs were confirmed with HE stains and α-synuclein immunohistochemistry. Out of the 39 cases, 33 showed LBAS in the olfactory bulb, 15 in the enteric nerve plexus, 23 in the sympathetic ganglia, and 16 in the pericardial nerve fibers of the left ventricle (Tables 3 and 4).

Olfactory mucosa

The olfactory epithelium is a pseudostratified columnar epithelium lying deep within the recess of the superior nasal cavity; it is composed of a mixture of multipotential stem cells (basal cells), supporting cells and olfactory receptor neurons (Fig. 2). Mature neurons are reported to give rise to fine and unmyelinated axons that ascend through the cribriform plate to synapse at glomeruli in the olfactory bulb.[20,45]

LBAS were found in the olfactory mucosa of seven (17.9%) out of 39 cases (Tables 3 and 4). These seven also had LBAS in the olfactory bulb. LBAS was present in the lamina propria mucosa of the seven cases (Fig. 4a–c). In addition, one case showed LBAS in a bundle of axons in the cribriform plate (Fig. 4d). None of the cases showed LBAS in the olfactory epithelial paraneuron. We summarized the demographic results of these seven individuals with LBAS in the olfactory mucosa in Table 5. Neither phosphorylated tau-positive deposits nor amyloid β immunopositive deposits were detected in the olfactory mucosa.

Table 3 The distribution of α-synuclein deposits in various anatomical regions of 39 cases with Lewy body disease

Age at death/gender	Parietal lobe	Frontal lobe	Temporal lobe	Cingulate gyrus	Entorhinal cortex	Amygdala	Olfactory bulb	Nucleus basalis of Meynert	Substantia nigra	Locus coeruleus	Dorsal motor nucleus of the vagus	Spinal Cord	Gastrointestinal system	Olfactory Mucosa	Sympathetic ganglion	Adrenal gland	Pericardial nerve	Skin	BBAR LB stage	NFT stage	SP stage
104/F																			5	4	C
70/F																			5	4	C
86/F																			5	6	C
84/M																			4	2	A
79/F																			4	2	A
80/F																			4	2	A
81/M																			3	2	A
88/M																			3	3	A
79/M																			2	1	A
68/F																			2	2	B
79/F																			2	6	C
77/F																			2	6	C
78/M																			1	2	A
75/M																			1	2	A
89/F																			1	3	C
93/F																			1	4	C
86/M																			1	4	C
81/M																			1	2	A
90/F																			1	2	A
86/M																			1	2	A
97/F																			1	2	A
78/M																			1	1	A
92/M																			1	3	C
94/M																			1	4	A
85/M																			1	3	A
81/F																			1	5	C
96/F																			1	2	0
87/F																			1	3	A
101/F																			1	4	A
69/F																			1	4	0
83/F																			1	3	A
72/M																			1	1	A
77/M																			1	2	A
83/M																			0.5	4	C
71/M																			0.5	2	A
89/M																			0.5	2	A
85/F																			0.5	3	A
85/F																			0.5	2	A
96/F																			0.5	3	A

Grade 0 = blank, grade 1 = light grey, grade 2 = light blue, grade 3 = blue, grade4 = navy blue. The number in each cell indicates a score based on the semiquantitative scoring system of Lewy-related pathology. 0 = neither Lewy neurites nor bodies detected by using anti-phosphorylated α-synuclein antibody. 1 = sparse phosphorylated α-synuclein immunopositive dots or neurites, neither Lewy bodies nor phosphorylated α-synuclein immunopositive intracytoplasmic aggregations. 2 = one to three Lewy bodies or phosphorylated α-synuclein immunopositive intracytoplasmic aggregations in a low-power field (×10). 3 = more than four Lewy bodies and scattered Lewy neurites in a low-power field (×10). 4 = numerous LBs and neurites with severe immunoreactivity for phosphorylated α-synuclein in the neuropil or background. Individuals of BBAR LB stages 3–5, with clinical Parkinsonism and neuropathologically numerous LBASs in the CNS, showed high incidence (75%, 6/8 individuals) of LBASs in the olfactory mucosa. In contrast, individuals of BBAR LB stages 1–3 without Parkinsonism showed extremely low incidence of Lewy body-related α-synucleinopathy (LBAS) (3%, 1/31) in the olfactory mucosa. LBAS was found in the olfactory mucosa mostly in advanced BBAR LB stages 3–5. BBAR LB Brain Bank for Aging Research Lewy body staging, NFT stage, Braak's stages for neurofibrillary tangles; SP stage, Braak's stages for senile plaques.

Table 4 Regional frequency of Lewy body-related α-synucleinopathy (LBAS) in various anatomical regions

The BBAR LB stage	Olfactory epithelium	Olfactory mucosa	Olfactory bulb	Spinal cord	GI tract	Sympathetic ganglia	Adrenal gland	Pericardial nerve	Skin
0.5	0/6	0/6	2/6	0/6	0/6	2/6	0/6	1/6	0/6
1	0/21	1/21	19/21	7/21	6/27	10/21	1/21	6/21	1/21
2	0/4	0/4	4/4	3/4	1/4	3/4	0/4	2/4	0/4
3	0/2	1/2	2/2	2/2	2/2	2/2	2/2	1/2	2/2
4	0/3	3/3	3/3	3/3	3/3	3/3	3/3	3/3	2/3
5	0/3	2/3	3/3	3/3	3/3	3/3	1/3	3/3	0/3
All	**0/39**	**7/39**	**33/39**	**18/39**	**15/39**	**23/39**	**7/39**	**16/39**	**5/39**

BBAR LB Brain Bank for Aging Research Lewy body staging.

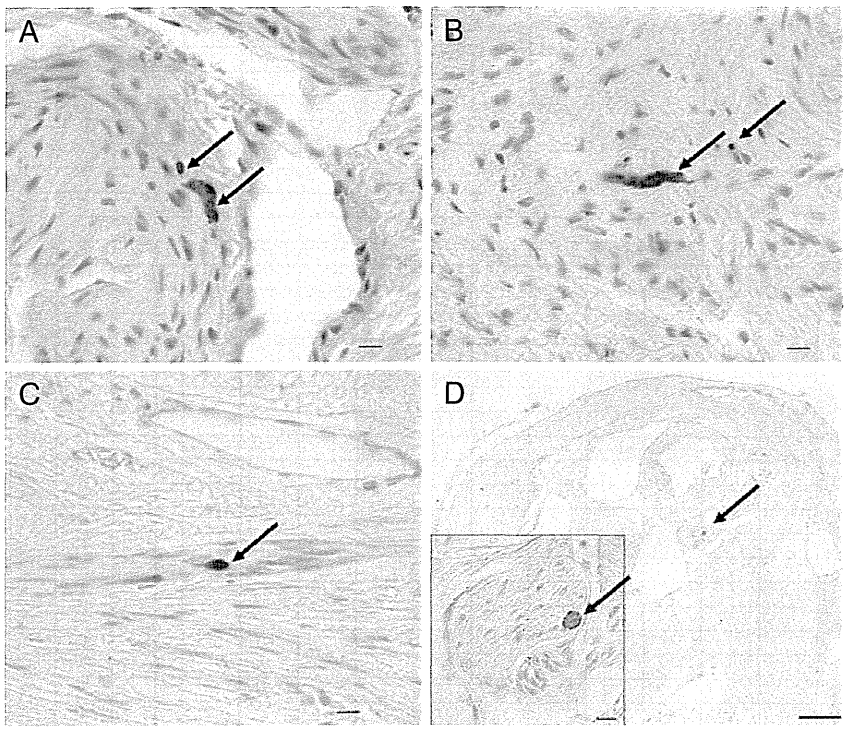

Fig. 4 Photomicrographs show α-synuclein immunopositive deposits (arrows indicate Lewy neurites) in the axonal bundle of the lamina propria (a–c) and cribriform plate (d). The inset in figure (d) shows a higher magnification image of α-synuclein immunopositive deposits in the axonal bundle of the cribriform plate. Immunohistochemistry using monoclonal antibody against phosphorylated α-synuclein (pSyn#64). Photomicrographs (a, b, c and d) were obtained from cases 4, 5, 7 and 3, respectively, in Table 5. (a–c), scale bar = 10 μm; (d) scale bar = 100 μm (inset, 10 μm).

Correlations between α-synuclein immunopositive LBs or LNs in the olfactory mucosa and CNS

Alpha-synuclein immunopositive LBs or LNs in the olfactory mucosa were detected in seven cases, including three with DLB, three with Parkinson's disease or Parkinson's disease with dementia, and one with incidental LBD (Tables 3–5). LBAS in the olfactory mucosa was compared with those in other locations of the CNS (Table 3). Individuals of BBAR LB stages 3–5, clinical and neuropathological diagnosis of LBD, showed a high incidence (75%, 6/8 individuals) of α-synuclein immunopositive LBAS in the olfactory mucosa (Table 6, Fig. 5). Six individuals with Parkinson's disease also showed a high incidence of α-synuclein accumulation (66%, 4/6 individuals) in the olfactory mucosa. In contrast, individuals of BBAR LB stages 0.5–2 (here we classified them into asymptomatic group) showed a low incidence of LBAS (3%, 1/31) in the olfactory mucosa.

Olfactory bulb

There is neural connectivity among olfactory receptor neurons and nuclei in the olfactory bulbs.[45] Hence, we analyzed the frequency of LBAS in the glomeruli, tufted cells, mitral cells and granular cells between LBAS-positive and LBAS-negative groups in the olfactory epithelium.

In individuals of BBAR LB stages 3–5 (symptomatic stage), LBAS was frequently observed in the glomeruli (8/8 cases, 100%), granular cells (8/8, 100%) and tufted cells (7/8, 87.5%). In contrast, there were low numbers of cases with LBAS in the mitral cells (2/8, 25%). Asymptomatic stage cases of LBD, corresponding to BBAR stage 0.5–2,

Table 5 Clinical and neuropathological demography of seven individuals with Lewy body-related α-synucleinopathy (LBAS) identified in the olfactory mucosa

No.	Age at death	Clinically diagnosed as LBD	Cause of death	Neuropathologic diagnosis	BBAR LB stage	LBAS in the olfactory mucosa			NFT stage	SP stage
						Olfactory epithelium	Lamina propria mucosa	Cribriform plate		
1	104/F	None	CHF, MI, Dementia	DLBN, AD	5	0	1	0	1	C
2	70/F	DLB	DLB, pneumonia	DLBN, AD	5	0	1	0	1	C
3	84/M	DLB	Prostate carcinoma, DLB	DLBL	4	0	1	1	2	A
4	79/F	PDD	PDD	PDDN	4	0	1	0	2	A
5	80/F	PD	Pneumonia, PD	PDDL	4	0	1	0	2	A
6	88/M	PD	Pneurmonia, PD	PD	3	0	1	0	2	A
7	86/M	None	Pneumonia	AD,Incidental LBD	1	0	1	0	1	C

AD, Alzheimer's disease; BBAR LB stage, Lewy body staging system of the Brain Bank for Aging Research; CHF, congestive heart failure; DLB, dementia with Lewy bodies; DLBL, dementia with Lewy bodies and a Lewy body score corresponding to the limbic form; DLBN, dementia with Lewy bodies and a Lewy body score corresponding to the neocortical form; F, female; LB, Lewy body; LBD, Lewy body disease; M, male; MI, acute myocardial infarction; NFT stage, Braak's stages for neurofibrillary tangles; PD, Parkinson's disease; PDDL, Parkinson's disease with dementia and a Lewy body score corresponding to the limbic form; PDDN, Parkinson's disease with dementia and a Lewy body score corresponding to the neocortical form; SP stage, Braak's stages for senile plaques.

Table 6 Incidence of LBAS in the olfactory mucosa in cases with symptomatic LBD (BBAR stage 3–5)

Clinical and neuropathologic diagnosis of LBD	LBAS in OM		Total
	Present	Absent	
Symptomatic (BBAR 3–5)	6*	2	8
Asymptomatic (BBAR 0.5–2)	1	30	31

*$P < 0.05$. BBAR, Brain Bank for Aging Research; LBAS; Lewy body-related alpha-synucleinopathy; LBD, Lewey body disease; OM; olfactory mucosa.

showed high incidence of LBAS in the glomeruli (23/31, 74.1%) and granular cells (22/31, 70.9%) of the olfactory bulb (Fig. 5).

DISCUSSION

Our study provides two novel observations.

1 LBAS in the olfactory mucosa was frequently observed (6/8 cases, 75%) in the symptomatic patients with LBD, but was a rare condition (1/31 cases, 3.2%) in asymptomatic LBD patients.
2 LBAS was seen in the glomeruli and granular cells in the olfactory bulbs of most symptomatic and asymptomatic cases with LBD.

It has been widely accepted that LB pathology does not develop simultaneously in all anatomical regions of the central and peripheral nervous systems. Hawkes *et al.* proposed that neurotropic pathogens may enter the brain via two routes: (i) a nasal route, with anterograde progression into the temporal lobe; and (ii) a gastric route secondary to the swallowing of nasal secretions in saliva (a dual hit hypothesis).[46] The former route may be associated with the early accumulation of α-synuclein in the human olfactory bulb and cause olfactory dysfunction in sporadic Parkinson's disease. In the present study, there was rare observation of LBAS in the olfactory mucosa in the asymptomatic cases of LBD. Further analysis is important to clarify the possibility of propagation of α-synuclein in the nervous systems.

In the present study, LBAS was frequently observed in the olfactory mucosa (6/8 cases, 75%) in the individuals with clinical LBD. In contrast, LBAS in the olfactory mucosa was a rare observation in asymptomatic patients. It is also important that all seven cases with LBAS in the olfactory mucosa had LBAS in the cerebral cortex and brainstem. Our results have similarities with a previous report concerning Alzheimer's disease.[20] Detection of LBAS in the olfactory mucosa could be hindered by two problems: technical difficulty in obtaining enough nerve fibers and rapid turnover of olfactory receptor neurons.[47,48] In fact, a recent study reported that a biopsy study revealed no α-synuclein immunopositive deposits in the olfactory

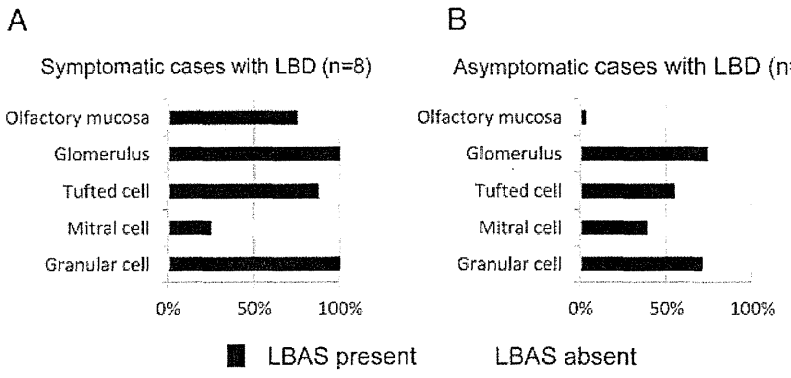

Fig. 5 Frequencies of cases having Lewy-related α-synucleinopathy (LBAS) pathology in the olfactory mucosa and each anatomical region of the olfactory bulb. (a) Cases with symptomatic dementia with Lewy bodies (LBD) ($n = 8$, Brain Bank for Aging Research [BBAR] stages 3–5). Most of the cases show LBAS pathology in the olfactory mucosa (6/8, 75%), glomeruli (8/8, 100%), tufted cells (6/7, 85.7%) and granular cells (8/8, 100%). The number of cases with LBAS in the mitral cells is low (2/6, 33.3%). (b) Cases with asymptomatic LBD ($n = 25$, BBAR stages 0.5–2). Most of the cases show LBAS pathology in the glomeruli (23/31, 74.1%), tufted cells (17/31, 54.8%) and granular cells (22/31, 70.9%). The number of cases with LBAS in the mitral cells (12/31, 38.7%) is low. LBAS pathology of the olfactory mucosa is present in only one case (1/31, 3.2%).

mucosa of patients of Parkinson's disease.[21] Our previous study indicated a high incidence of α-synuclein immunopositive LBs or neurites in aging human olfactory bulbs, and suggested that they extend from the periphery (the second olfactory structure) to the anterior olfactory nucleus (the tertiary olfactory structure).[11] The present study, using 6 μm-thick paraffin embedded sections, revealed that LBAS was most frequently observed in the glomeruli which were composed of axon terminals of olfactory epithelial cells and dendrites of mitral and tufted cells[45] as well as in the glomerular cells which were most numerous in the periphery of the olfactory bulb (Fig. 5). We consider that high incidence of LBAS in glomeruli may represent affected terminal axons of olfactory epithelial neurons. In contrast to our result, a previous study, employing 50 μm-thick floating sections, reported high frequency of LBAS in mitral cells and the internal plexiform layer in individuals with Parkinson's disease but no LBAS in age-matched controls.[49] Further studies are necessary to identify the most vulnerable subset in the periphery of the olfactory bulb.

In conclusion, presence of LBAS in the olfactory mucosa and olfactory glomeruli further supports the importance of olfactory system as an entry zone of LBD. Future studies of LB pathology involving the olfactory system are indicated to understand the pathomechanism of α-synuclein accumulation in individuals with LBD.

ACKNOWLEDGMENTS

This study was supported in part by a Grant-in-Aid for Scientific Research (Kakenhi B) (20390248) (SM), The Specified Disease Treatment Research Program (SM), Research on Measures for Intractable Diseases (MT) (H23-nanchi-ippan-062, H24-nanchi-ippan-063, Nanchi-ippan-013), and the Comprehensive Brain Science Network (SM, MT). We gratefully acknowledge Naoo Aikyo, Fumio Hasegawa, Mieko Harada, Yuki Kimura, Nobuko Naoi and Sachiko Imai for technical help. We thank Dr. T. Iwatsubo (Department of Neuropathology, University of Tokyo, Tokyo, Japan) for the kind gifts of antibodies and Dr. K. Suzuki (Department of Neuropathology, Tokyo Metropolitan Geriatric Hospital and Institute of Gerontology) for useful discussions and comments.

Portions of this study were presented at the 86th annual meeting of the American Association of Neuropathologists, Philadelphia, in 2010.

REFERENCES

1. Baba M, Nakajo S, Tu PH *et al.* Aggregation of alpha-synuclein in Lewy bodies of sporadic Parkinson's disease and dementia with Lewy bodies. *Am J Pathol* 1998; **152**: 879–884.
2. Spillantini MG, Crowther RA, Jakes R, Hasegawa M, Goedert M. alpha-Synuclein in filamentous inclusions of Lewy bodies from Parkinson's disease and dementia with Lewy bodies. *Proc Natl Acad Sci U S A* 1998; **95**: 6469–6473.
3. Goedert M, Spillantini MG, Davies SW. Filamentous nerve cell inclusions in neurodegenerative diseases. *Curr Opin Neurobiol* 1998; **8**: 619–632.
4. Ogunnyi A, Akang EE, Gureje O *et al.* Dementia with Lewy bodies in a Nigerian: a case report. *Int Psychogeriatr* 2002; **14**: 211–218.
5. Takao M, Ghetti B, Yoshida H *et al.* Early-onset dementia with Lewy bodies. *Brain Pathol* 2004; **14**: 137–147.
6. Braak H, Ghebremedhin E, Rub U, Bratzke H, Del Tredici K. Stages in the development of Parkinson's disease-related pathology. *Cell Tissue Res* 2004; **318**: 121–134.
7. Braak H, Sastre M, Bohl JR, de Vos RA, Del Tredici K. Parkinson's disease: lesions in dorsal horn layer I,

involvement of parasympathetic and sympathetic pre- and postganglionic neurons. *Acta Neuropathol* 2007; **113**: 421–429.
8. Braak H, Braak E. Pathoanatomy of Parkinson's disease. *J Neurol* 2000; **247** (Suppl 2): II3–I10.
9. Braak H, Del Tredici K, Rub U, de Vos RA, Jansen Steur EN, Braak E. Staging of brain pathology related to sporadic Parkinson's disease. *Neurobiol Aging* 2003; **24**: 197–211.
10. Del Tredici K, Rub U, De Vos RA, Bohl JR, Braak H. Where does Parkinson disease pathology begin in the brain? *J Neuropathol Exp Neurol* 2002; **61**: 413–426.
11. Sengoku R, Saito Y, Ikemura M *et al.* Incidence and extent of Lewy body-related alpha-synucleinopathy in aging human olfactory bulb. *J Neuropathol Exp Neurol* 2008; **67**: 1072–1083.
12. Ponsen MM, Stoffers D, Booij J, van Eck-Smit BL, Wolters ECh, Berendse HW. Idiopathic hyposmia as a preclinical sign of Parkinson's disease. *Ann Neurol* 2004; **56**: 173–181.
13. Haehner A, Boesveldt S, Berendse HW *et al.* Prevalence of smell loss in Parkinson's disease – a multicenter study. *Parkinsonism Relat Disord* 2009; **15**: 490–494.
14. Daniel SE, Hawkes CH. Preliminary diagnosis of Parkinson's disease by olfactory bulb pathology. *Lancet* 1992; **340** (8812): 186.
15. Pearce RK, Hawkes CH, Daniel SE. The anterior olfactory nucleus in Parkinson's disease. *Mov Disord* 1995; **10**: 283–287.
16. Beach TG, White CL 3rd, Hladik CL *et al.* Olfactory bulb alpha-synucleinopathy has high specificity and sensitivity for Lewy body disorders. *Acta Neuropathol* 2009; **117**: 169–174.
17. Parkkinen L, Silveira-Moriyama L, Holton JL, Lees AJ, Revesz T. Can olfacotry bulb biopsy be justified for the diagnosis of Parkinson's disease? Comments on 'olfactory bulb α-synucleinopathy has specificity and sensitivity for Lewy body disorders'. *Acta Neuropathol* 2009; **117** (2): 213–214.
18. Jellinger KA. Olfactory bulb α-synucleinopathy has specificity and sensitivity for Lewy body disorders. *Acta Neuropathol* 2009; **117** (2): 215–216.
19. Duda JE, Shah U, Arnold SE, Lee VM, Trojanowski JQ. The expression of alpha-, beta-, and gamma-synucleins in olfactory mucosa from patients with and without neurodegenerative diseases. *Exp Neurol* 1999; **160**: 515–522.
20. Arnold SE, Lee EB, Moberg PJ *et al.* Olfactory epithelium amyloid-beta and paired helical filament-tau pathology in Alzheimer disease. *Ann Neurol* 2010; **67**: 462–469.
21. Witt M, Bormann K, Gudziol V *et al.* Biopsies of olfactory epithelium in patients with Parkinson's disease. *Mov Disord* 2009; **24**: 906–914.
22. Fumimura Y, Ikemura M, Saito Y *et al.* Analysis of the adrenal gland is useful for evaluating pathology of the peripheral autonomic nervous system in Lewy body disease. *J Neuropathol Exp Neurol* 2007; **66**: 354–362.
23. Saito Y, Ruberu NN, Sawabe M *et al.* Staging of argyrophilic grains: an age-associated tauopathy. *J Neuropathol Exp Neurol* 2004; **63**: 911–918.
24. Saito Y, Ruberu NN, Sawabe M *et al.* Lewy body-related alpha-synucleinopathy in aging. *J Neuropathol Exp Neurol* 2004; **63**: 742–749.
25. Saito Y, Kawashima A, Ruberu NN *et al.* Accumulation of phosphorylated alpha-synuclein in aging human brain. *J Neuropathol Exp Neurol* 2003; **62**: 644–654.
26. Ikemura M, Saito Y, Sengoku R *et al.* Lewy body pathology involves cutaneous nerves. *J Neuropathol Exp Neurol* 2008; **67**: 945–953.
27. McKeith IG, Galasko D, Kosaka K *et al.* Consensus guidelines for the clinical and pathologic diagnosis of dementia with Lewy bodies (DLB): report of the consortium on DLB international workshop. *Neurology* 1996; **47**: 1113–1124.
28. Folstein MF, Folstein SE, McHugh PR. 'Mini-mental state'. A practical method for grading the cognitive state of patients for the clinician. *J Psychiatr Res* 1975; **12**: 189–198.
29. Hasegawa K Inoue K, Moriya K. An investigation of dementia rating scale for the elderly. *Seishin Igaku* 1974; **16**: 965–969.
30. Hosokawa T, Yamada Y, Isagoda A, Nakamura R. Psychometric equivalence of the Hasegawa Dementia Scale-Revised with the Mini-Mental State Examination in stroke patients. *Percept Mot Skills* 1994; **79**: 664–666.
31. Lawton MP, Brody EM. Assessment of older people: self-maintaining and instrumental activities of daily living. *Gerontologist* 1969; **9**: 179–186.
32. Morris JC. The Clinical Dementia Rating (CDR): current version and scoring rules. *Neurology* 1993; **43**: 2412–2414.
33. McKhann G, Drachman D, Folstein M, Katzman R, Price D, Stadlan EM. Clinical diagnosis of Alzheimer's disease: report of the NINCDS-ADRDA Work Group under the auspices of Department of Health and Human Services Task Force on Alzheimer's Disease. *Neurology* 1984; **34**: 939–944.
34. McKeith IG, Dickson DW, Lowe J *et al.* Diagnosis and management of dementia with Lewy bodies: third report of the DLB Consortium. *Neurology* 2005; **65**: 1863–1872.

35. Gallyas F. Silver staining of Alzheimer's neurofibrillary changes by means of physical development. *Acta Morphol Acad Sci Hung* 1971; **19**: 1–8.
36. Fujiwara H, Hasegawa M, Dohmae N *et al.* alpha-Synuclein is phosphorylated in synucleinopathy lesions. *Nat Cell Biol* 2002; **4**: 160–164.
37. Braak H, Braak E. Neuropathological stageing of Alzheimer-related changes. *Acta Neuropathol* 1991; **82**: 239–259.
38. Braak H, Alafuzoff I, Arzberger T, Kretzschmar H, Del Tredici K. Staging of Alzheimer disease-associated neurofibrillary pathology using paraffin sections and immunocytochemistry. *Acta Neuropathol* 2006; **112**: 389–404.
39. Murayama S, Saito Y. Neuropathological diagnostic criteria for Alzheimer's disease. *Neuropathology* 2004; **24**: 254–260.
40. Consensus recommendations for the postmortem diagnosis of Alzheimer's disease. The National Institute on Aging, and Reagan Institute Working Group on Diagnostic Criteria for the Neuropathological Assessment of Alzheimer's Disease. *Neurobiol Aging* 1997; **18**: S1–S2.
41. Hyman BT, Trojanowski JQ. Consensus recommendations for the postmortem diagnosis of Alzheimer disease from the National Institute on Aging and the Reagan Institute Working Group on diagnostic criteria for the neuropathological assessment of Alzheimer disease. *J Neuropathol Exp Neurol* 1997; **56**: 1095–1097.
42. Jellinger KA. Dementia with grains (argyrophilic grain disease). *Brain Pathol* 1998; **8**: 377–386.
43. Jellinger KA, Bancher C. Senile dementia with tangles (tangle predominant form of senile dementia). *Brain Pathol* 1998; **8**: 367–376.
44. Kosaka K. Diffuse neurofibrillary tangles with calcification: a new presenile dementia. *J Neurol Neurosurg Psychiatry* 1994; **57**: 594–596.
45. Hawkes CH, Doty RL. *The Neurology of Olfaction.* Cambridge, UK: Cambridge University Press, 2009; 16–21.
46. Hawkes CH, Del Tredici K, Braak H. Parkinson's disease: a dual-hit hypothesis. *Neuropathol Appl Neurobiol* 2007; **33**: 599–614.
47. Graziadei PP, Okano M. Neuronal degeneration and regeneration in the olfactory epithelium of pigeon following transection of the first cranial nerve. *Acta Anat (Basel)* 1979; **104**: 220–236.
48. Graziadei PP, Monti Graziadei AG. Regeneration in the olfactory system of vertebrates. *Am J Otolaryngol* 1983; **4**: 228–233.
49. Ubeda-Bañon I, Saiz-Sanchez D, de la Rosa-Prieto C, Argandoña-Palacios L, Garcia-Muñozguren S, Martinez-Marcos A. alpha-Synucleinopathy in the human olfactory system in Parkinson's disease: involvement of calcium-binding protein- and substance P-positive cells. *Acta Neuropathol* 2010; **119**: 723–735.

Neurobiology of Disease

Accumulation of α-Synuclein Triggered by Presynaptic Dysfunction

Yasuto Nakata,[1,4] Toru Yasuda,[1,4,5] Masahiro Fukaya,[2] Saori Yamamori,[3] Makoto Itakura,[3] Tomoko Nihira,[1,4] Hideki Hayakawa,[1,4] Aya Kawanami,[1] Masakazu Kataoka,[6] Makiko Nagai,[1] Hiroyuki Sakagami,[2] Masami Takahashi,[3] Yoshikuni Mizuno,[4] and Hideki Mochizuki[1,4,5]

Departments of [1]Neurology, [2]Anatomy, and [3]Biochemistry, and [4]Division of Neuroregenerative Medicine, Kitasato University School of Medicine, Sagamihara, Kanagawa 252-0374, Japan, [5]Department of Neurology, Osaka University Graduate School of Medicine, Suita, Osaka 565-0871, Japan, and [6]Department of Environmental Science and Technology, Faculty of Engineering, Shinshu University, Nagano-shi, Nagano 380-8553, Japan

Pathological examination of dementia with Lewy bodies patients identified the presence of abnormal α-synuclein (αSyn) aggregates in the presynaptic terminals. αSyn is involved in the regulation of soluble *N*-ethylmaleimide-sensitive factor attachment protein receptor (SNARE) complex. Importantly, αSyn-transgenic mouse and postmortem examination of patients with Parkinson's disease have demonstrated the abnormal distribution of SNARE protein in presynaptic terminals. In this study, we investigated the effects of SNARE dysfunction on endogenous αSyn using *Snap25*$^{S187A/S187A}$ mutant mice. These mice have homozygous knock-in gene encoding unphosphorylatable S187A-substituted synaptosomal-associated protein of 25 kDa (SNAP-25). The mice displayed a significant age-dependent change in the distribution of αSyn and its Ser^{129}-phosphorylated form in abnormally hypertrophied glutamatergic nerve terminals in the striatum. Electron-microscopic analysis revealed the abnormally condensed synaptic vesicles with concomitant mislocalization of αSyn protein to the periactive zone in the glutamatergic nerve terminals. However, the *Snap25*$^{S187A/S187A}$ mutant mouse harbored no abnormalities in the nigrostriatal dopaminergic neurons. Our present results suggest that SNARE dysfunction is the initial trigger of mislocalization and accumulation of αSyn, and probably is an important pathomechanism of α-synucleinopathies.

Introduction

α-Synucleinopathies are a subgroup of neurodegenerative diseases including dementia with Lewy bodies (DLB), multiple system atrophy (MSA), and Parkinson's disease (PD). The pathological hallmark of the disorders is the formation of intracellular aggregates composed mainly of α-synuclein (αSyn), which are called Lewy bodies and Lewy neurites (Spillantini and Goedert, 2000; Galvin et al., 2001; Yasuda et al., 2012). It was reported recently that >90% of αSyn aggregates are present in presynaptic terminals in the form of very small deposits of the affected neurons in DLB (Neumann et al., 2002; Kramer and Schulz-Schaeffer, 2007; Schulz-Schaeffer, 2010). However, the mechanisms responsible for presynaptic accumulation of abnormal αSyn remain elusive.

Received May 8, 2012; revised Aug. 28, 2012; accepted Oct. 5, 2012.

Author contributions: Y.N., T.Y., and H.M. designed research; Y.N., T.Y., M.F., S.Y., M.I., T.N., H.H., and A.K. performed research; Y.N., T.Y., M.F., S.Y., M.I., T.N., H.H., A.K., M.K., M.N., H.S., M.T., Y.M., and H.M. analyzed data; Y.N. and T.Y. wrote the paper.

This work was supported by Grants from the Japan Science and Technology Agency, Core Research for Evolutional Science and Technology (H.M.); Grants-in-Aid from the Research Committee of CNS Degenerative Diseases, the Ministry of Health, Labour and Welfare of Japan (H.M.); Grant-in-Aid for Research on Applying Health Technology (H23–015) from the Ministry of Health, Labour and Welfare of Japan (H.M.); Ministry of Education, Culture, Sports, Science and Technology of Japan Grant S0801035 (H.M.); and Grant-in-Aid for Scientific Research on Innovative Areas (Brain Environment) from the Ministry of Education, Science, Sports and Culture of Japan (H.M.).

The authors declare no competing financial interests.

Correspondence should be addressed to Prof. Hideki Mochizuki, Department of Neurology, Osaka University Graduate School of Medicine, 2-2 Yamadaoka, Suita, Osaka 565-0871, Japan. E-mail: hmochizuki@neurol.med.osaka-u.ac.jp.

DOI:10.1523/JNEUROSCI.2220-12.2012

 0270-6474/12/3217186-11$15.00/0

Generally, αSyn is abundantly localized in the presynaptic nerve terminals (Maroteaux et al., 1988; Iwai et al., 1995). While the physiological functions of αSyn have yet to be defined, several lines of evidence implicated this protein in the modulation of neurotransmitter release through the regulation of formation of the soluble *N*-ethylmaleimide-sensitive factor attachment protein receptor (SNARE) complex (Chandra et al., 2005; Burré et al., 2010; Darios et al., 2010) and the size of synaptic vesicle pool (Murphy et al., 2000; Cabin et al., 2002; Larsen et al., 2006; Nemani et al., 2010). Vesicle-associated membrane protein-2 (VAMP-2) present in the synaptic vesicles, and syntaxin and synaptosomal-associated protein of 25 kDa (SNAP-25) in the presynaptic plasma membrane form the core SNARE complex, which regulate the docking and fusion of synaptic vesicles to the presynaptic membrane (Südhof, 2004). A recent study showed the physical interaction of αSyn with VAMP-2 to promote SNARE assembly (Burré et al., 2010). Cysteine-string protein-α (CSPα) also participates in SNARE assembly, and mutant mice lacking CSPα displayed impaired SNARE formation and premature death, but both of these phenotypes are counteracted by transgenic expression of αSyn (Chandra et al., 2005; Sharma et al., 2011). However, overexpression of αSyn with no overt toxicity inhibits neurotransmitter release, due to a defective reclustering of synaptic vesicles after endocytosis (Nemani et al., 2010). Additionally, overexpressed αSyn indirectly inhibited SNARE-mediated exocytosis by sequestering arachidonic acid, which upregulates syntaxin and enhances its engagement with SNARE complex (Darios et al., 2010). Importantly, abnormal redistribu-

tion of SNARE proteins has been observed in human PD patients and mice overexpressing a truncated form of human αSyn, which showed decreased release of dopamine (DA) in the striatum (Garcia-Reitböck et al., 2010). Therefore, presynaptic SNARE dysfunction is considered an initial pathogenic event in α-synucleinopathies.

Based on the above background, the present study was designed to investigate the effects of impaired SNARE assembly on the distribution of naive αSyn. We exploited *Snap25*$^{S187A/S187A}$ mutant mice. This strain is resistant to the protein kinase C-mediated phosphorylation of SNAP-25 at Ser^{187} and represents a concomitant reduction of neurotransmitter release, including serotonin and DA, from the amygdala, and develops convulsive seizures and anxiety-related behavior in general activity and light-and-dark preference tests (Kataoka et al., 2011). The results indicated that dysfunction of SNARE proteins could trigger abnormal localization and accumulation of presynaptic αSyn, possibly representing one of the pathogenic events in DLB or MSA.

Materials and Methods

Mice. All experimental protocols described in this study were approved by the Animal Experimentation and Ethics Committee of the Kitasato University School of Medicine. Homozygous SNAP-25 knock-in mutant mice bearing S187A mutation and wild-type littermate control mice were generated based on the procedures described in detail by Kataoka et al. (2011). Briefly, embryonic stem cells with the heterozygous *Snap25*^{S187A} mutant allele were generated and microinjected into C57BL/6N blastocysts to obtain heterozygous mutant mice. Male chimeras were bred with C57BL/6N female mice. After the line was backcrossed 13 times, homozygous mice (designated as *Snap25*$^{S187A/S187A}$ mice) were obtained by *in vitro* fertilization. The genotype was checked by PCR. In this experiment, wild-type and *Snap25*$^{S187A/S187A}$ mice were used at age 11 (females), 54 (females), 60 (males), and 61 (females) weeks.

Tissue processing. Deeply anesthetized mice (with 250 mg/kg, i.p., sodium pentobarbital) were perfused transcardially with PBS or with 2% paraformaldehyde/2% glutaraldehyde in 0.1 M phosphate buffer (PB). The brains were removed en bloc from the skull and cut sagittally into two brain hemispheres for confocal microscopy, cell counting, electron microscopy, Western blotting, and catecholamine analysis. Tissue processing for conventional electron microscopy is described below (see Conventional electron microscopy). For confocal microscopy and cell counting, hemisphere brain blocks of mice perfused transcardially with PBS or with 2% paraformaldehyde/2% glutaraldehyde in 0.1 M PB were fixed overnight in 4% paraformaldehyde in PBS and immersed in PBS containing 30% sucrose until sinking. Coronal sections of the striatum and the entire rostrocaudal extent of the substantia nigra (SN) were cut serially at 20 μm thickness using a cryostat (CM1850; Leica Microsystems). For Western blotting and catecholamine measurement by HPLC, brain blocks of mice perfused transcardially with PBS were dissected using the method described previously by our group, to yield the striatal tissues and ventral parts of midbrain tissues including the SN (Yasuda et al., 2011). After completing the dissection, the sections were immediately frozen on dry ice and stored at −80°C until analysis.

Antibodies. The primary antibodies used for confocal microscopy were mouse anti-αSyn (clone 42; diluted at 1:100; BD Biosciences) (Tapia-González et al., 2011), rabbit anti-αSyn (1:500; Millipore Bioscience Research Reagents) (Chung et al., 2003; Herzig et al., 2011), rabbit anti-tyrosine hydroxylase (TH) (1:5000; Calbiochem) (Yasuda et al., 2011), mouse anti-synaptophysin (clone SY38; 1:500; Millipore) (Masliah et al., 2001; Tabuchi et al., 2007; Gimbel et al., 2010), rat anti-dopamine transporter (DAT) (clone MAB369; 1:500; Millipore) (Herzig et al., 2011; Kaushal et al., 2011), rabbit or goat anti-vesicular glutamate transporter-1 (VGLUT1) (1:300; Frontier Institute) (Miyazaki et al., 2003; Kawamura et al., 2006), goat anti-VGLUT2 (1:300; Frontier Institute) (Miyazaki et al., 2003; Kawamura et al., 2006), and rabbit anti-Ser^{129}-phosphorylated αSyn (ab59264; 1:100; Abcam) (Pan-Montojo et al., 2010; Yasuda et al., 2011). For Western blotting, primary antibodies used were mouse anti-αSyn (clone 42; 1:150; BD Biosciences), rabbit anti-Ser^{129}-phosphorylated αSyn (ab59264; 1:500; Abcam), rabbit anti-SNAP25ct (1:1000) (Yamamori et al., 2011), mouse anti-syntaxin 1 (10H5) (1.4 μg/ml) (Yamamori et al., 2011), rabbit anti-VAMP-2 (1.4 μg/ml) (Kataoka et al., 2011), mouse anti-synaptophysin (clone SY38; 1:500; Millipore), rabbit anti-TH (1:500; Calbiochem), and rabbit anti-β-tubulin (1:500; Abcam). For immunoelectron microscopy, the primary antibodies used were mouse anti-αSyn (clone 42; 1 μg/ml; BD Biosciences), guinea pig anti-DAT (1 μg/ml; Frontier Institute), and rabbit anti-VGLUT1 (1 μg/ml; Frontier Institute).

Confocal microscopy. Free-floating sections were washed in PBS medium containing 0.05% Triton X-100 (PBS-T). As to the sections prepared from mice perfused transcardially with 2% paraformaldehyde/2% glutaraldehyde in 0.1 M PB, they were incubated with Liberate Antibody Binding (L.A.B.) solution (Polysciences) followed by washing in PBS medium and then processed in the same way as other sections. The sections were soaked with blocking agents and then incubated with the primary antibody dissolved in dilution reagent at 4°C for 48 h. Vector M.O.M. Immunodetection Kit (Vector Laboratories) was used for blocking and antibody dilution according to the instructions provided by the manufacturer. Subsequently, for fluorescent visualization of the antigens, the sections were incubated for 2 h in fresh medium containing fluorescein isothiocyanate-conjugated anti-mouse or rabbit IgG, and Cy3-conjugated anti-mouse, rabbit, goat, or rat IgG secondary antibodies (1:200–500; Jackson ImmunoResearch Laboratories). The sections were mounted on slide glass and coverslipped with Vectashield Mounting Medium with or without DAPI (Vector Laboratories). Images were captured using a confocal laser-scanning microscope (model LSM510; Zeiss) equipped with ZEN 2009 software (Zeiss) with identical settings. The software was used for image processing (brightness and contrast adjustment) applied equally to the images of wild-type and mutant mice.

Conventional electron microscopy. For conventional electron microscopy, the hemisphere brains prepared from mice perfused transcardially with 2% paraformaldehyde/2% glutaraldehyde in 0.1 M PB were post-fixed in 2% OsO_4 for 1 h. After washing in water, the samples were incubated in 2% uranyl acetate for 30 min. After dehydration using 50, 70, 90, and 100% ethanol solutions and 100% propylene oxide, the samples were embedded in Epon 812 resin (Nissin EM). Ultrathin sections were obtained using a Leica Ultracut UCT and stained with 2% uranyl acetate and lead citrate. Electron micrographs were taken with an H-7650 electron microscope (Hitachi).

Immunoelectron microscopy. For preembedding immunoelectron microscopy, parasagittal brain sections (60 μm in thickness) were incubated successively with 5% normal goat serum, primary antibodies, and peroxidase- or coloidal gold (1.4 nm)-conjugated secondary antibodies (Invitrogen). Immunoreaction was visualized with 3,3′-diaminobenzidine or silver enhancement kit (HQ silver; Nanoprobes). When combining the two methods for double immunoelectron microscopy, the brain tissue was subjected first to immunoperoxidase and then to silver-enhanced immunogold. Sections labeled by immunoperoxidase and silver-enhanced immunogold were subjected to electron microscopy as described above. The size of the nerve terminal was quantitated by using the ImageJ 1.43 software (Wayne Rasband, NIH, Bethesda, MD; http://rsb.info.nih.gov/ij).

Western blotting. Frozen striatal and ventral midbrain tissues were sonicated in chilled CelLytic-MT mammalian tissue lysis/extraction reagent (Sigma-Aldrich) mixed with protease inhibitor mixture set I (Calbiochem) and phosphatase inhibitor mixture set V (Calbiochem). The samples were centrifuged (20,000 × *g* for 10 min at 4°C), and the resulting supernatants were collected and used for Western blotting. The protein concentration in the lysate of all samples was determined using BCA protein assay kit (Pierce). Each protein sample (5–15 μg) was resolved by SDS-PAGE by means of Compact-PAGE-twin (ATTO) and then electrotransferred to Clear Blot Membrane-P (ATTO) using powered BLOT-mini (ATTO). The membrane was washed in PBS-T, incubated for 1 h in PBS-T containing 50% ChemiBLOCKER (Millipore), and then incubated for 24 h with the primary antibody in the same fresh medium. Subsequently, the membrane was incubated for 2 h in fresh medium containing horseradish peroxidase-linked anti-mouse or rabbit IgG secondary antibody (1:10,000–20,000; GE Healthcare), followed by devel-

opment of chemiluminescence using GE Healthcare ECL Plus Western Blotting Detection System (GE Healthcare). The image was captured using LAS-4000 (Fujifilm), and the signal intensity was quantitated using the ImageJ 1.43 software.

Assay for SNARE complex assembly. SNARE complex assembly was assessed by measuring the levels of the high-molecular-weight SDS-resistant complex in Western blotting performed without boiling of the samples before gel electrophoresis (Hu et al., 2002; Asuni et al., 2008; Sakisaka et al., 2008). Striatal lysate samples (15 μg of protein/sample) of wild-type and *Snap25*$^{S187A/S187A}$ mice were resolved in the SDS sample buffer. Samples were incubated for 20 min at room temperature and were further incubated at room temperature or boiled at 100°C for 3 min. Subsequently, they were analyzed by SDS-PAGE followed by the immunoblotting using the rabbit anti-SNAP25ct primary antibody (1:1000) (Yamamori et al., 2011) and horseradish peroxidase-linked anti-rabbit IgG secondary antibody (1:10,000; GE Healthcare). Except for the sample preparation before gel electrophoresis, all procedures were the same as described above (see Western blotting).

Determination of striatal levels of DA and its metabolites by HPLC. Frozen striatal tissues were sonicated in 50 mM sodium acetate. The samples were centrifuged (20,000 × *g* for 10 min at 4°C), and the resulting supernatants were mixed with equal volumes of 0.2N perchloric acid. The samples were centrifuged (20,000 × *g* for 10 min at 4°C), and the resulting supernatants were subjected to measurement of DA, homovanillic acid (HVA), and 2-(3,4-dihydroxyphenyl)-acetic acid (DOPAC) concentrations by HPLC, using an HPLC system equipped with electrochemical detection (ECD-100; EICOM; applied voltage, 500 mV) and reverse-phase column (TSK gel ODS-80TM; Tosoh). The HPLC system consisted of a pump (PU-980; Jasco; flow rate, 1.0 ml/min), autosampler (AS-1550; Jasco), column oven (860-CO; Jasco), and degasser (DG-2080–53 Jasco). The mobile phase consisted of a solution, pH 3.72, containing the following: 0.085 M $NaH_2PO_4 \cdot 2H_2O$, 2.5 mM 1-octanesulfonic acid sodium salt, 20 μM EDTA-2Na, and 15% methanol. The concentrations of DA, HVA, and DOPAC were determined in nanomoles per gram of tissue weight, and the results were expressed relative to the values of wild-type mice.

Cell count. For DA cell counting in the SN pars compacta (SNpc), every fourth 20-μm-thick serial section of the brain was immunostained for TH and counterstained with cresyl violet (Nissl staining) (Furuya et al., 2004; Yasuda et al., 2011). The numbers of TH- and Nissl-double-positive cells in the SNpc were counted both in wild-type and *Snap25*$^{S187A/S187A}$ mice in a blind manner. The SNpc cells that have nuclei optimally visible by TH immunostaining, and nuclei, cytoplasm, and nucleoli prominently stained by Nissl staining were counted. To avoid double counting of neurons with unusual shapes, TH- and Nissl-double-positive cells were counted only when their nuclei and nucleoli were optimally visualized. The rostral end of the SNpc was determined to the level where TH- and Nissl-double-positive cells began to appear (~2.60 mm caudal to the level of the bregma) (Franklin and Paxinos, 2008), and the caudal end of the SNpc was defined to the level where TH- and Nissl-double-positive cells and oculomotor nerves can be observed (~3.80 mm caudal to the level of the bregma) (Yasuda et al., 2011). In the rostral half region of the SN (~2.60–3.16 mm caudal to the level of the bregma), the SNpc was distinguished from medial ventral tegmental area (VTA) by the vertical line extended from the medial end of the cerebral peduncle. In the caudal region of the SN where the medial lemniscus can be observed (~3.16–3.80 caudal to the level of the bregma), the SNpc and medial VTA were divided along the medial lemniscus.

Statistical analysis. All data are expressed as mean ± SEM, excluding those of VGLUT1-positive nerve area, which are expressed as mean ± SD. The two-tailed Student's *t* test (for two groups) was applied. A value of $p < 0.05$ denoted the presence of statistically significant difference.

Results

Abnormal distribution of αSyn protein at presynaptic terminals in the striatum of *Snap25*$^{S187A/S187A}$ mice

Using immunohistochemistry, we investigated the distribution of endogenous αSyn in the striatum of *Snap25*$^{S187A/S187A}$ mice, which have unphosphorylatable Ala at position Ser^{187} in the SNAP-25 protein. A significant decrease of neurotransmitter release was noted in serotonergic and dopaminergic systems in the amygdala, which was associated with behavioral abnormalities, including spontaneous convulsive seizures (Kataoka et al., 2011). Confocal microscopic analysis of the striatal sections of the *Snap25*$^{S187A/S187A}$ mice showed altered distribution of endogenous αSyn, which resembled coarse granular deposits, at the age of 11 weeks, compared with age-matched wild-type control. These changes were prominent in 60-week-old (54-week-old or more was designated as aged, hereafter) *Snap25*$^{S187A/S187A}$ mice (Fig. 1*A*,*B*), indicating an age-dependent progressive manner of redistribution.

Next, we examined the localization of αSyn in the presynaptic terminals by using anti-synaptophysin antibody. Aged *Snap25*$^{S187A/S187A}$ mice showed similar alternation of the immunoreactivity for synaptophysin as observed for αSyn, compared with the wild-type (Fig. 1*C*,*D*). Moreover, αSyn-immunopositive granular structures were largely overlapped with synaptophysin. These results indicate that αSyn accumulates mainly in the presynaptic terminals in the striatum. We also analyzed the immunostaining pattern for Ser^{129}-phosphorylated αSyn (p-αSyn), which was found specifically in human α-synucleinopathies (Fujiwara et al., 2002). Majority of αSyn-positive granular deposits were immunopositive for p-αSyn, which were detected at negligible amounts in wild-type control mice (Fig. 1*F*,*G*). These results indicate that the abnormal accumulation of αSyn in the striatum of *Snap25*$^{S187A/S187A}$ mice represents in part the pathological changes in human DLB brains.

Abnormal accumulation of αSyn and p-αSyn proteins in the striatum of *Snap25*$^{S187A/S187A}$ mice

Next, we measured αSyn and p-αSyn protein levels in the striatal tissues of aged *Snap25*$^{S187A/S187A}$ mice. A significant decrease of SNAP-25 protein was found in *Snap25*$^{S187A/S187A}$ mice ($p < 0.0001$) compared with age-matched wild-type mice, confirming our previous findings (Kataoka et al., 2011). Importantly, αSyn (~1.5-fold; $p = 0.0047$) and p-αSyn (~1.7-fold; $p = 0.0080$) protein levels were higher than age-matched wild-type mice (Fig. 2*A*,*B*). These results indicate that the abnormal distribution of αSyn and p-αSyn in the presynaptic terminals (Fig. 1*F*) was reflected by increased amount of these proteins. In addition, high levels of VAMP-2 (~1.3-fold; $p = 0.0011$), but neither syntaxin nor synaptophysin, were found in the striatum of aged *Snap25*$^{S187A/S187A}$ mice (Fig. 2*A*,*B*), compared with whole-brain lysate prepared from young *Snap25*$^{S187A/S187A}$ mice (Kataoka et al., 2011).

Ultrastructural analysis of αSyn distribution in presynaptic terminals

To investigate in detail the morphological changes in the presynaptic terminals, we used electron microscopy to analyze the striatum of the aged mice. In *Snap25*$^{S187A/S187A}$ mice, condensed synaptic vesicles were abundantly present in large excitatory nerve terminals, compared with the normal uniform distribution of the vesicles in wild-type mice (Fig. 3*A*,*B*). These results suggest possible decrease of presynaptic neurotransmitter release in *Snap25*$^{S187A/S187A}$ mice. Subsequent immunoelectron-microscopic examination of αSyn in the synapses showed predominant localization of αSyn proteins in the periactive zone of enlarged excitatory presynaptic nerve terminals in the aged *Snap25*$^{S187A/S187A}$ mice, compared with the wild type (Fig. 3*C*,*D*).

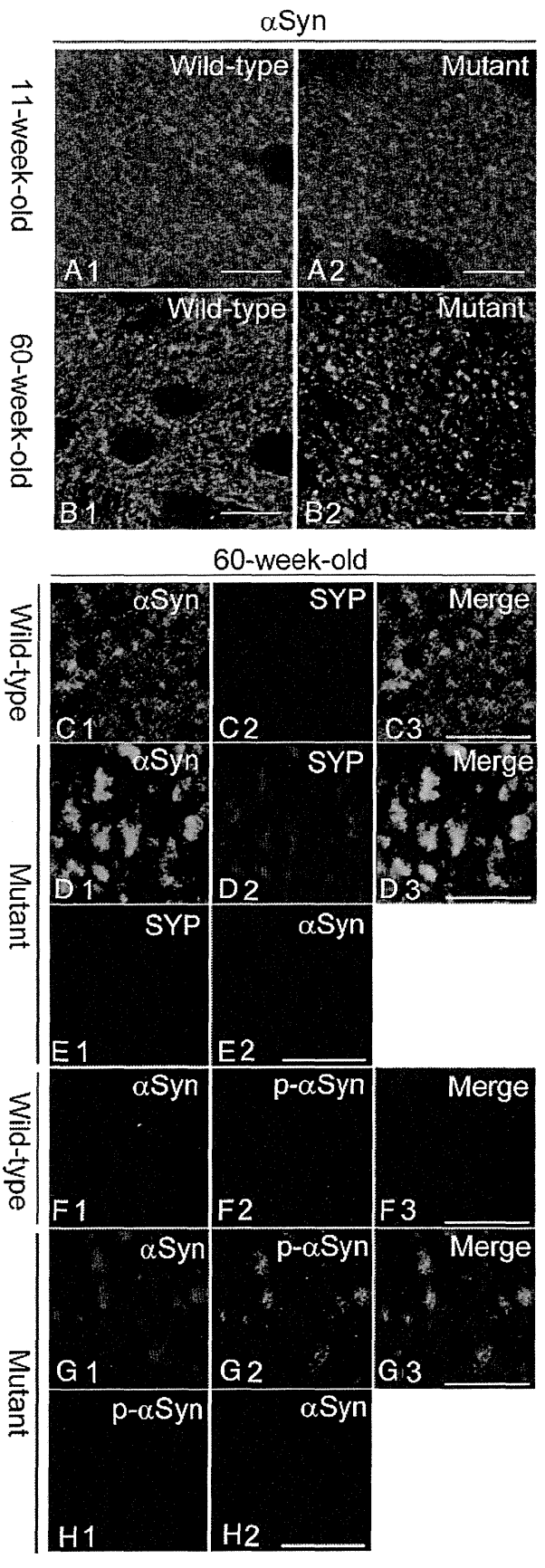

Figure 1. Altered localization of αSyn and its accumulation in presynaptic terminals in the striatum of *Snap25*$^{S187A/S187A}$ mice. ***A***, ***B***, Striatal sections of wild-type and *Snap25*$^{S187A/S187A}$ (mutant) mice at postnatal weeks 11 and 60 were immunostained for αSyn ($n = 3$ for each genotype). Compared with the wild-type mice (A_1, B_1), αSyn was localized and formed coarse granular deposits in mutant mice at postnatal weeks 11 and 60 (A_2, B_2). The severity of the change was more prominent at postnatal week 60. Scale bars, 10 μm. ***C–H***, Sections were coimmunostained for αSyn, and synaptophysin (SYP) or p-αSyn. Confocal images showed altered localization of SYP (D_2) and p-αSyn (G_2) and colocalization with αSyn-positive coarse granular deposits (D_1, G_1) in mutant mice (D_3, G_3). No cross-reactivity was observed for the sections of the mutant mice exposed to a single primary antibody followed by the treatment of both secondary antibodies were observed (E_1, E_2; H_1, H_2) [i.e., negligible green (E_1) and red fluorescence (E_2) for the sections treated with anti-SYP and αSyn antibody, respectively]. Scale bars, 5 μm.

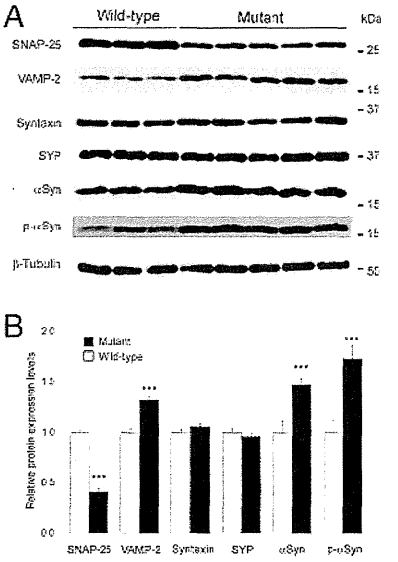

Figure 2. Increase in endogenous αSyn and p-αSyn in the striatum of *Snap25*$^{S187A/S187A}$ mice. ***A***, ***B***, Western blotting was performed for synaptic marker proteins using the striatal tissues at postnatal week 61. ***A***, Representative Western blotting images of two to five independent experiments, each involving three and five mice for wild-type and *Snap25*$^{S187A/S187A}$ (mutant), respectively. Mutant mice showed increased band intensity of αSyn, p-αSyn, and VAMP-2 compared with the wild type, while that of SNAP-25 was decreased. ***B***, Relative protein expression levels expressed relative to the loading control (β-tubulin). The band intensity was quantitated using the ImageJ 1.43 software and expressed as the relative protein expression level. Significant increases in α-Syn, p-αSyn, and VAMP-2, and significant decrease in SNAP-25 were observed in mutant mice. No significant differences were noted in other synaptic protein markers. Data are mean ± SEM of two to five independent experiments, each involving three and five mice for wild-type and mutant, respectively. ***$p < 0.01$ (two-tailed t test).

Decreased ability of SNARE complex assembly in *Snap25*$^{S187A/S187A}$ mice

Given that *Snap25*$^{S187A/S187A}$ mice clearly displayed the significant decrease in the SNAP-25 protein expression and abnormal distribution of the synaptic vesicle in the presynaptic terminals (Figs. 2, 3*B*), we evaluated the functional ability to produce the SNARE complex in *Snap25*$^{S187A/S187A}$ mice. SNARE complex assembly was assessed by measuring the levels of the high-molecular-weight heat-sensitive SDS-resistant complex in Western blotting. As shown in Figure 4*A*, compared with boiled sample of the wild type, SNAP-25-immunoreactive bands were shifted to the higher molecular masses (~75 to ~250 kDa) in unboiled samples of wild-type and *Snap25*$^{S187A/S187A}$ mice. However, the relative signal intensity of higher molecular masses normalized by β-tubulin (loading control) was significantly reduced in *Snap25*$^{S187A/S187A}$ mice, compared with the wild-type mice ($p = 0.00463$) (Fig. 4*B*). These observations indi-

cated the decreased ability of the SNARE complex assembly in *Snap25*$^{S187A/S187A}$ mice compared with the wild-type mice. This is considered to represent the functional deficit possibly attributable to the decreased level of the SNAP-25 and the insensitivity of protein kinase C-mediated phosphorylation at Ser^{187} in *Snap25*$^{S187A/S187A}$ mice.

αSyn accumulation and enlargement of corticostriatal nerve terminals

The striatal spiny interneurons receive excitatory outputs from cortical and thalamic tracts, and these projections use glutamate as the neurotransmitter (Gerfen and Surmeier, 2011). VGLUT1 and VGLUT2 are localized to the excitatory nerve terminals projecting from the cortical and the thalamic area, respectively, in the striatum. Then, we investigated the distribution of αSyn-immunopositive deposits with VGLUT1 or VGLUT2 to verify the abnormal accumulation of αSyn in the corticostriatal or the thalamostriatal neuronal terminals. As shown in Figure 5B_2, we found similar alternation of the immunoreactivity for VGLUT1 as observed for αSyn in the aged *Snap25*$^{S187A/S187A}$ mice compared with wild-type normal ones (Fig. 5A_2). Importantly, such immunoreactivity for VGLUT1, but not for VGLUT2, was exclusively colocalized with αSyn (Fig. 5B_3,E_3). We also performed double immunostaining with anti-pSyn and anti-VGLUT1 antibodies and found the VGLUT1-immunopositive structures to be immunopositive for p-αSyn (Fig. 5G_3). These observations suggest accumulation of αSyn and p-αSyn mainly in the enlarged VGLUT1-positive nerve terminals.

Immunoelectron-microscopic examination showed massive enlargement of the VGLUT1-positive nerve terminals in the aged *Snap25*$^{S187A/S187A}$ mice (Fig. 5*I*,*J*). Quantitative analysis of the size of the VGLUT1-positive nerve terminals based on the cumulative probability curve confirmed a significantly larger size in *Snap25*$^{S187A/S187A}$ mice compared with wild-type mice (Fig. 5*K*). The size of the VGLUT1-positive nerve terminals reached a plateau at 0.8 μm^2 in wild-type mice, while that of *Snap25*$^{S187A/S187A}$ mice reached a plateau at 3.6 μm^2. The size of ~40% of the VGLUT1-positive nerve terminals in the mutant mice was larger than the maximum size measured in wild-type mice. Specifically, the size of the VGLUT1-positive nerve terminals in the mutant mice was approximately fourfold larger than the wild type (p = 0.0030) (Fig. 5*L*).

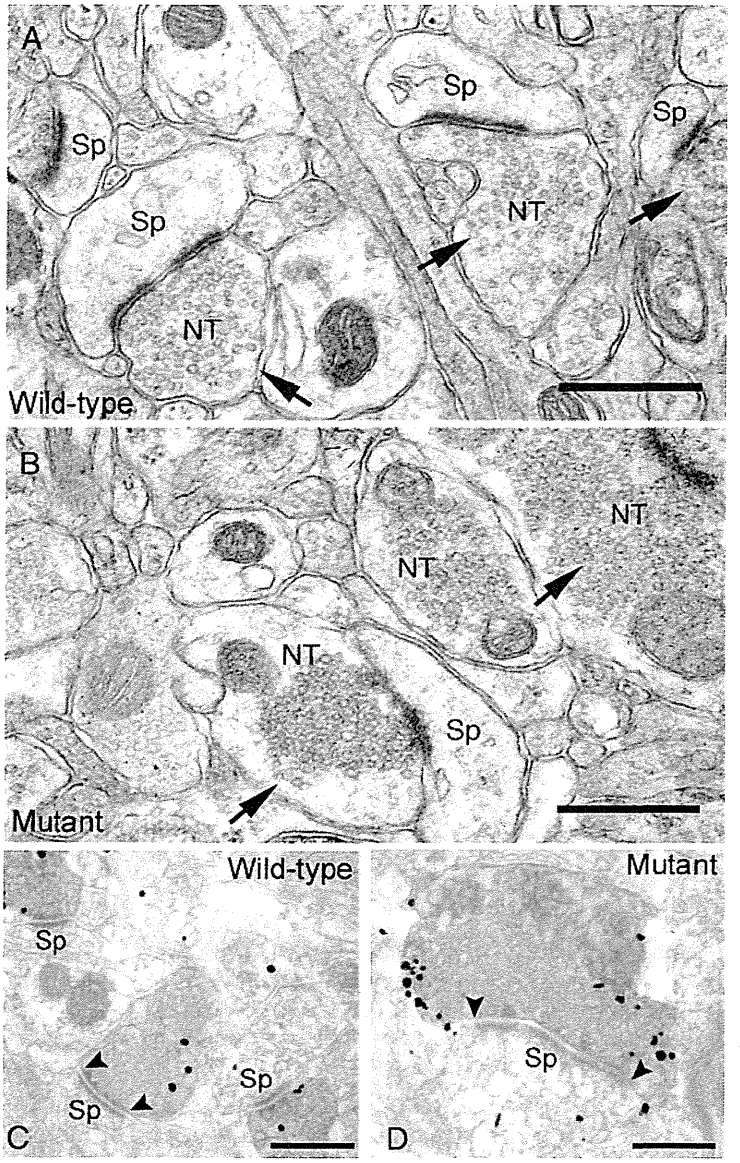

Figure 3. Abnormal excitatory nerve terminals in the striatum of *Snap25*$^{S187A/S187A}$ (mutant) mice. Representative electron micrographs of wild-type and mutant mice at postnatal week 60 (n = 3 for each genotype). Synaptic vesicles were homogeneously distributed in the cytoplasm of the excitatory nerve terminals in wild-type mice (***A***), while they were tightly assembled in mutant mice (***B***). Note the alteration of subcellular localization of α-Syn (immunogold particles) and increased number of αSyn aggregates deposited in association with the cytoplasmic face of the plasma membrane at the periactive zone of the enlarged nerve terminals in mutant mice (***D***), but not in wild-type mice (***C***). Arrows, excitatory nerve terminals; arrowheads, edges of active zone. NT, Nerve terminal; Sp, dendritic spine. Scale bars, 500 nm.

No significant changes in nigrostriatal dopaminergic system

Finally, we examined the effect of SNARE dysfunction on the nigrostriatal dopaminergic system, which is affected in parkinsonian brains. The striatal sections of aged *Snap25*$^{S187A/S187A}$ mice were coimmunostained for αSyn and dopaminergic neuronal markers (TH or DAT). The αSyn-immunopositive deposits appeared adjacent to, but hardly colocalized with both DAT and TH in *Snap25*$^{S187A/S187A}$ mice. The distribution patterns of DAT- and TH-immunoreactive deposits in the striatum were not significantly different between wild-type and mutant mice (Fig. 6*A–D*). These results imply that the nigrostriatal dopaminergic neurons are not affected in *Snap25*$^{S187A/S187A}$ mice.

To clarify this point further, we conducted immunoelectron-microscopic examination of DAT-positive dopaminergic nerve terminals. There were no significant differences in any structural alternations including condensation of synaptic vesicles (Fig. 6*E*,*F*). Furthermore, we found no significant differences in the subcellular localization of αSyn protein between the aged wild-type and *Snap25*$^{S187A/S187A}$ mice (Fig. 6*G*,*H*).

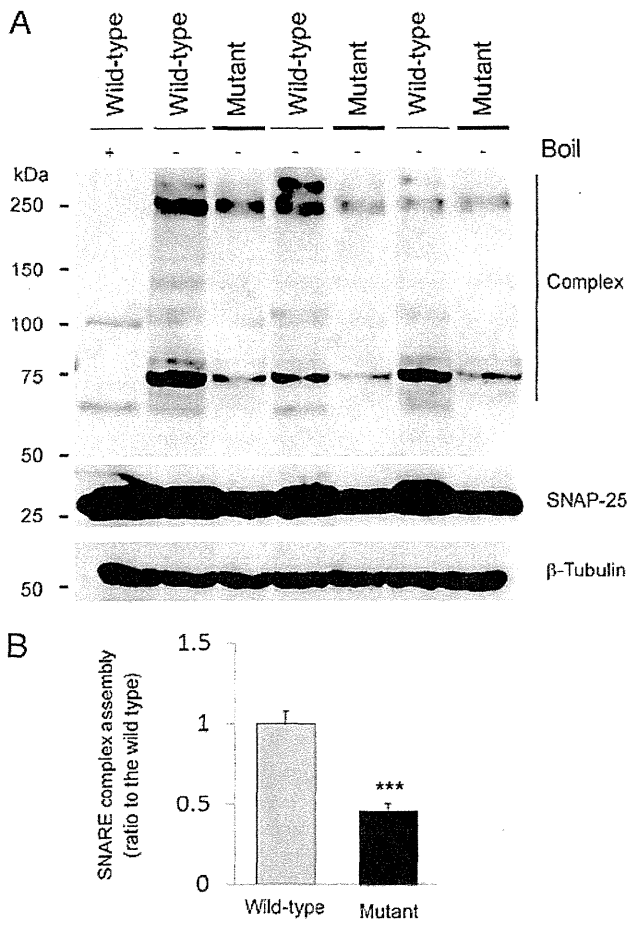

Figure 4. Decreased ability of the SNARE complex assembly in *Snap25*$^{S187A/S187A}$ (mutant) mice. ***A***, ***B***, Western blotting was performed for unboiled or boiled samples of wild-type and mutant mice (at postnatal week 61) before electrophoresis followed by the immunoblotting using SNAP-25ct antibody. ***A***, Representative Western blotting image of two to three independent experiments was provided. Heat-sensitive SDS-resistant SNAP-25ct-immunoreactive bands were detected at high molecular mass (~75 to ~250 kDa) in wild-type and mutant mice, indicating the presence of the SNARE complex. However, band intensity of the mutant mice, especially at ~75 kDa, was decreased compared with the wild-type mice. ***B***, Relative levels of the SNARE complex assembly relative to the loading control (β-tubulin). The band intensity was quantitated using the ImageJ 1.43 software and expressed as the relative protein expression level. Significant decrease in SNARE complex assembly was observed in mutant mice compared with the wild-type mice. Data are mean ± SEM of two to three independent experiments, each involving three mice for each genotype. ***$p < 0.01$ (two-tailed t test).

We also investigated the functional preservation of the nigrostriatal dopaminergic neurons in the aged *Snap25*$^{S187A/S187A}$ mice. No significant difference was found in the number of TH- and Nissl-double-positive cells in the SNpc between wild-type and *Snap25*$^{S187A/S187A}$ mice (Fig. 6*I*,*J*). There were also no significant differences in the levels of TH protein in the midbrain tissue and DA and its metabolites, HVA and DOPAC, in the striatum between the aged wild-type and *Snap25*$^{S187A/S187A}$ mice (Fig. 6*K*–*M*). These results suggest that SNARE dysfunction does not seem to be involved in the initiation of PD-related pathologic changes in nigrostriatal dopaminergic neurons.

Discussion

In this study, we found that SNARE dysfunction leads to presynaptic accumulation of endogenous αSyn, a process that probably represents the initial pathological event in DLB. Previous studies using neural preparations showed that the neurotransmitter release is regulated by protein kinase C, which phosphorylates Ser^{187} residue in SNAP-25, augmenting exocytosis of synaptic vesicles (Majewski and Iannazzo, 1998; Morgan et al., 2005). Patch-clamp analysis of chromaffin cells that overexpress the S187A form of SNAP-25 inhibited the rate of refilling of presynaptic vesicle pool (Nagy et al., 2002). Recently, we reported that *Snap25*$^{S187A/S187A}$ mice show reduced DA and serotonin release in amygdala (Kataoka et al., 2011). In human DLB brains, >90% of αSyn aggregates are located in the presynaptic terminals in the form of small deposits (Neumann et al., 2002; Kramer and Schulz-Schaeffer, 2007; Schulz-Schaeffer, 2010). This is consistent with the present findings of abnormal accumulation of αSyn in presynapses, suggesting that this process is the initial pathological event in DLB, eventually leading to the death and degeneration of neuronal cells (Orimo et al., 2008). Another finding that lends support to the role of αSyn aggregates in the presynaptic terminals in DLB was the lack of histopathological changes in the dopaminergic terminals in the present study.

In experiments on glutamate release conducted in hippocampal slices prepared from αSyn knock-out mice (Gureviciene et al., 2007), paired-pulse facilitation was significantly weaker, and high-frequency-induced long-term potentiation and frequency facilitation were not observed. These findings suggest that αSyn contributes to mobilization of glutamate-containing vesicles from the reserve pool (Gureviciene et al., 2007). Thus, αSyn may act as a positive regulator of neurotransmitter release at presynaptic terminals. Therefore, presynaptic accumulation of αSyn observed in *Snap25*$^{S187A/S187A}$ mice might reflect a compensatory response to a possible SNARE dysfunction-related chronic shortage of neurotransmitter release in the VGLUT1-positive nerve terminals.

In the striatum, the medium spiny neurons, which constitute >90% of all striatal neurons, receive output from glutamatergic axons that contact the spine head and dopaminergic axons that synapse with the dendritic spine neck. DA released from dopaminergic axons regulates the release of glutamate via D_2-like receptors on the corticostriatal nerve terminals (Bamford et al., 2004; Wickens and Arbuthnott, 2005). In the present study, we found no significant changes in the striatal tissue levels of DA and its metabolites. These findings confirmed the results reported in our previous study using *Snap25*$^{S187A/S187A}$ mice, whereas microdialysis analysis study revealed marked reduction of DA release from the amygdala (not measured in other brain regions) (Kataoka et al., 2011). In addition, in another *in vitro* study using PC12 cells, phosphorylation of SNAP-25 at S187 potentiated calcium-dependent DA release and recruitment of synaptic vesicles containing DA (Shimazaki et al., 1996; Iwasaki et al., 2000; Shoji-Kasai et al., 2002). These observations suggest decreased striatal DA release in *Snap25*$^{S187A/S187A}$ mice, resulting in increased demand for neurotransmitter release at glutamatergic nerve terminals. Thus, presynaptic accumulation of αSyn might reflect a possible compensatory response to low DA inhibitory control over cortical glutamatergic drive.

Increased expression of VAMP-2 protein accompanied increased αSyn expression in the striatum of *Snap25*$^{S187A/S187A}$ mice. Binding of the C terminus of αSyn to the N terminus of VAMP-2 primes the subsequent SNARE complex assembly (Burgoyne and Morgan, 2011). Therefore, the increased VAMP-2 level might also reflect a compensatory response to the impaired synaptic vesicle release by enhancing SNARE complex formation in concert with the increased αSyn.

Presynaptic neurotransmitter release is mediated by the synaptic vesicle cycle, consisting of exocytosis followed by en-

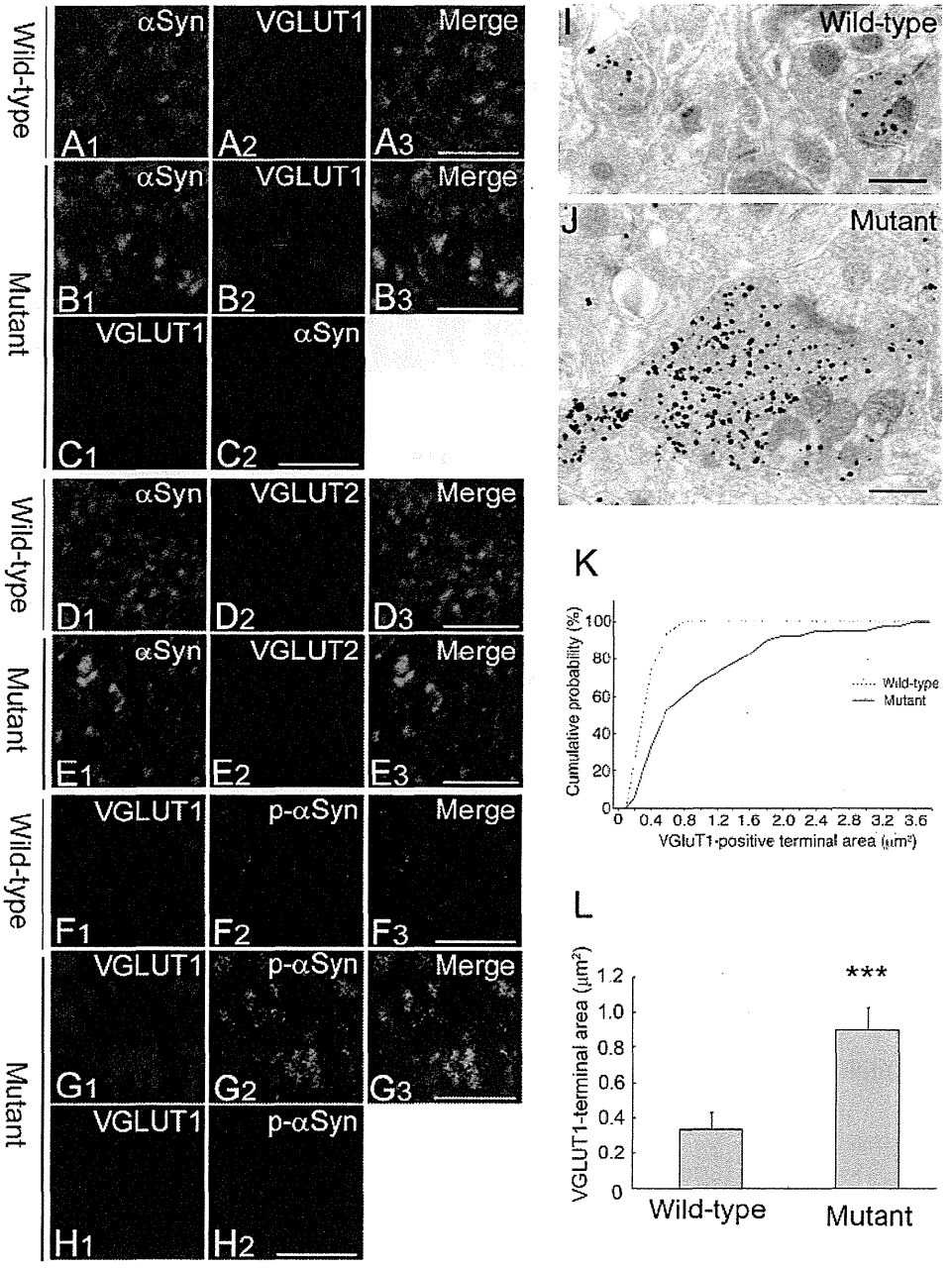

Figure 5. Accumulation of αSyn in the hypertrophied VGLUT1-positive nerve terminals. ***A–E***, Striatal sections of wild-type and *Snap25*$^{S187A/S187A}$ (mutant) mice at postnatal week 60 were coimmunostained for αSyn (green) and VGLUT1 or VGLUT2 (red) ($n = 3$ for each genotype). Confocal images showed altered localization of VGLUT1 with more granular appearance in mutant mice (***B***$_2$) compared with wild-type mice (***A***$_2$). Immunopositive structures for VGLUT1, but not for VGLUT2, marked colocalization with αSyn-positive granular deposits (***B***$_3$, ***E***$_3$). No cross-reactivity was observed for the sections of the mutant mice treated with a single antibody followed by both the secondary antibodies, as evidenced by negligible green (***C***$_1$) and red fluorescence (***C***$_2$) for the sections treated with anti-VGLUT1 and αSyn antibody, respectively. Scale bars, 5 μm. ***F–H***, Sections were coimmunostained for VGLUT1 (red) and p-αSyn (green) ($n = 3$ for each genotype). Confocal images showed marked colocalization of VGLUT1 and p-αSyn in mutant mice (***G***$_3$). Similarly, no cross-reactivity was observed as evidenced by negligible red (***H***$_1$) and green fluorescence (***H***$_2$) for the sections treated with anti-VGLUT1 and αSyn antibody, respectively. Scale bars, 5 μm. ***I, J***, Representative electron micrographs showing VGLUT1-positive nerve terminals (labeled with immunogold particles). Note the hypertrophy of VGLUT1-positive nerve terminals in mutant mice (***J***), but not in wild-type mice (***I***). Scale bars, 500 nm. ***K, L***, Quantitative analysis of VGLUT1-positive nerve terminal area in three mice per group. The size was measured in 100 nerve terminals per animal. Cumulative probability (***K***) and group mean value (***L***) were calculated and showed a larger nerve terminal area in mutant mice than the wild type. Data are mean ± SD. ***$p < 0.01$ (two-tailed t test).

docytosis and recycling. Exocytosis incorporates synaptic vesicles into the presynaptic terminal membranes and increases the surface area, while endocytosis retrieves the excess plasma membrane components followed by recycling to form other synaptic vesicles. Under normal conditions, the dynamics of the balance between exocytosis and endocytosis is well preserved to maintain the correct surface area of the presynaptic terminal (Hayes and Baines, 1996; Haucke et al., 2011). However, excessive accumulation of presynaptic vesicles and enlargement of the VGLT1-positive nerve terminals was observed in *Snap25*$^{S187A/S187A}$ mice. Taking into consideration the synaptic vesicle cycle, our findings suggest that the balance of the cycle was biased toward decreased exocytosis concomitant with possible decreased endocytosis.

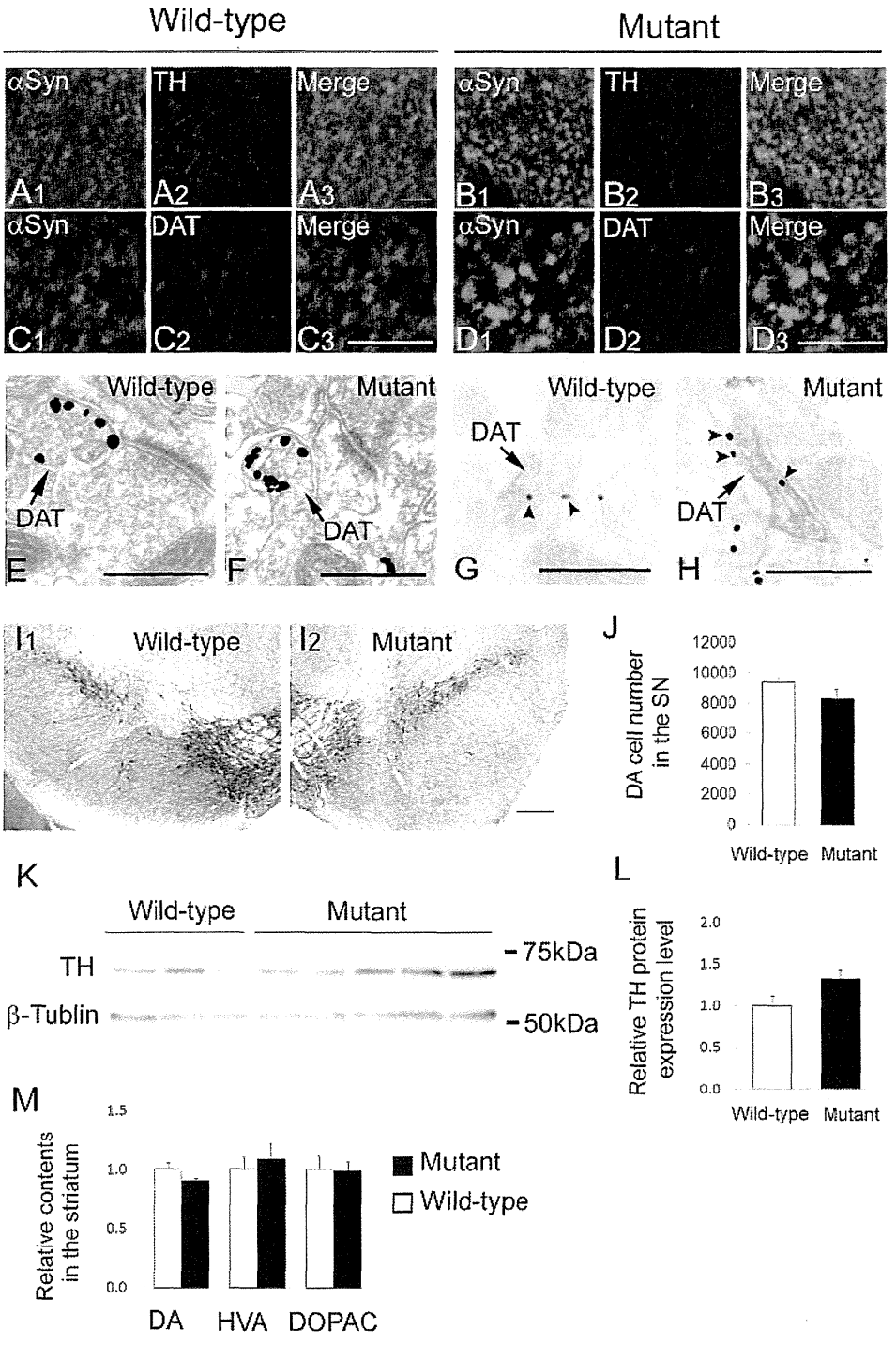

Figure 6. Lack of neurodegenerative changes in nigrostriatal dopaminergic neurons. ***A–D***, Striatal sections of wild-type and *Snap25*$^{S187A/S187A}$ (mutant) mice at postnatal week 60 were coimmunostained for α-Syn (green) and TH or DAT (red) ($n = 3$ for each genotype). There were no significant differences in the distribution pattern of TH (***A***$_2$, ***B***$_2$) and DAT (***C***$_2$, ***D***$_2$) between wild-type and mutant mice. αSyn-positive granular deposits (***B***$_1$, ***D***$_1$) were rarely colocalized with TH or DAT (***B***$_3$, ***D***$_3$). Scale bars, 5 μm. ***E–H***, Representative electron micrographs of dopaminergic nerve terminals at postnatal week 60 ($n = 3$ for each genotype). They were identified by silver particles (***E***, ***F***) or DAB labeling (***G***, ***H***) for DAT (arrows). There were no significant differences in subcellular localization of synaptic vesicles (***E***, ***F***) or αSyn (arrowheads, silver particles) (***G***, ***H***) between wild-type and mutant mice. Scale bars, 500 nm. ***I***, ***J***, Representative micrographs of the substantia nigra of wild-type and mutant mice at postnatal week 60 immunostained for TH and counterstained with cresyl violet. Scale bars: ***I***$_1$, ***I***$_2$, 200 μm. Number of DA cell bodies counted in three mice of each genotype. Data are mean ± SEM (***J***). ***K***, ***L***, Western blotting was performed using substantia nigral tissues at postnatal week 61. Representative images of Western blotting from two independent experiments, each involving three and five mice of wild-type and mutant mice, respectively (***K***). Relative TH protein expression levels (relative to the expression of β-tubulin) were expressed relative to the value of wild-type mice (***L***). Data are mean ± SEM of two independent experiments, each involving three and five mice of wild-type and mutant, respectively. ***M***, Quantification of DA, HVA, and DOPAC levels in the striatum of mice at postnatal week 54. Data were expressed relative to those of wild-type mice and represent the mean ± SEM of duplicate measurement of one experiment involving four mice of each genotype. There were no significant differences between wild-type and mutant mice (***J***, ***L***, ***M***) (two-tailed *t* test).

The enlarged VGLUT1-positive nerve terminals of *Snap25*$^{S187A/S187A}$ mice showed concomitant accumulation of αSyn and p-αSyn. Kramer and Schulz-Schaeffer (2007) have previously reported that 90% or even more of αSyn aggregates in DLB cases were located at the presynapses in the form of very small deposits. In parallel, dendritic spines were retracted, whereas the presynapses were relatively preserved, suggesting that a neurotransmitter deprivation may explain the cognitive impairment in DLB (Kramer and Schulz-Schaeffer, 2007; Schulz-Schaeffer, 2010). While the presynaptic aggregates did not contain much p-αSyn in their examination (Kramer and Schulz-Schaeffer, 2007; Schulz-Schaeffer, 2010), widespread varicosities and dot-like structures containing p-αSyn are commonly observed in mouse model and human DLB brains (Saito et al., 2003; Scott et al., 2010). This may represent axonal transport defects and presynaptic dysfunctions (Saito et al., 2003; Scott et al., 2010). Recent study showed that mutant αSyn (A53T) diminished levels of various motor proteins in neurons (Chung et al., 2009), supporting this scenario. Alternatively, excessive amounts of misfolded αSyn and p-αSyn may aggregate at synapses, physically preventing the targeting of other presynaptic proteins (Kramer and Schulz-Schaeffer, 2007). In experiments using *Caenorhabditis elegans* overexpressing the human αSyn, four genes related to the endocytosis process were identified as genetic modifiers for αSyn toxicity (Kuwahara et al., 2008). They included the two subunits of the adaptor protein (AP) complex 2, which interacts with clathrin and promotes presynaptic clathrin-mediated vesicle recycling (Morgan et al., 2000). Furthermore, proteomics analysis revealed that p-αSyn also preferentially interacted with the proteins involved in endocytosis, including clathrin heavy chain and subunit of AP-2 and AP-1 complexes, over the nonphosphorylated αSyn (McFarland et al., 2008). Clathrin-mediated recycling of exocytosed synaptic vesicles occurs in the periactive zone, a region adjacent to the active zone where synaptic vesicle is endocytosed (Haucke et al., 2011). Similarly, in *Snap25*$^{S187A/S187A}$ mice, immunoelectron microscopy showed preferential localization of αSyn at the periactive zone of the excitatory presynaptic nerve terminals (Fig. 3*D*). This might reflect the interaction of αSyn and p-αSyn with the proteins involved in clathrin-mediated endocytosis. Taking these findings together, presynaptic accumulation of αSyn and p-αSyn could disturb the endocytosis process and consequently contribute to the development of VGLUT1-positive terminal enlargement.

Presynaptic accumulation of αSyn is considered an early event in the pathogenesis of α-synucleinopathies (Neumann et al., 2002; Kramer and Schulz-Schaeffer, 2007; Schulz-Schaeffer, 2010). Mice overexpressing human αSyn showed presynaptic accumulation of αSyn and low DA release in the striatum. These findings were associated with abnormal distribution of SNARE proteins, which colocalized with αSyn aggregates. Similarly, accumulation of SNARE proteins and αSyn were reported in the striatum of PD patients (Garcia-Reitböck et al., 2010). These observations suggest that SNARE dysfunction likely occurs at an early stage of pathogenesis in nigrostriatal dysfunction observed in PD. By considering the findings observed in the VGLUT1-positive nerve terminals, we expected that SNARE dysfunction might have induced presynaptic accumulation of αSyn, which consequently results in the development of neurodegenerative changes in the nigrostriatal system. However, contrary to our expectation, *Snap25*$^{S187A/S187A}$ mice showed no significant neurodegenerative changes in nigrostriatal dopaminergic neurons, suggesting that SNARE dysfunction alone was insufficient to cause nigrostriatal degeneration as observed in PD, and appeared to be a downstream event associated with abnormal accumulation of αSyn.

In conclusion, the present study demonstrated that SNARE dysfunction leads to accumulation of endogenous αSyn in the corticostriatal nerve terminals. Presynaptic accumulation of αSyn is considered to be a key early event in the pathogenesis of α-synucleinopathies. Although the "prion-like" propagation hypothesis of αSyn, including tau and TAR DNA-binding protein 43 kDa, is currently receiving considerable attention worldwide, our findings provide an insight to our understanding of the possible mechanisms that lead to presynaptic accumulation of endogenous αSyn. Moreover, given that SNAP-25 is reduced in the striatum of MSA brains (Tong et al., 2010), we speculate that a discontinuous pattern of αSyn pathologies usually found in MSA [i.e., glial cytoplasmic inclusions in the putaminal oligodendrocytes, and neuronal cytoplasmic inclusions and neuronal nuclear inclusions in the cortex (Yoshida, 2007; Ubhi et al., 2011)] might be potentially linked through the presynaptic accumulation of αSyn in the corticostriatal neurons. Further investigations on the *Snap25* mutant mice with genetic ablation of αSyn would contribute to understanding the essential role of redistributed αSyn and should be a central issue in the following studies.

References

Asuni AA, Cunningham C, Vigneswaran P, Perry VH, O'Connor V (2008) Unaltered SNARE complex formation in an in vivo model of prion disease. Brain Res 1233:1–7. CrossRef Medline

Bamford NS, Robinson S, Palmiter RD, Joyce JA, Moore C, Meshul CK (2004) Dopamine modulates release from corticostriatal terminals. J Neurosci 24:9541–9552. CrossRef Medline

Burgoyne RD, Morgan A (2011) Chaperoning the SNAREs: a role in preventing neurodegeneration? Nat Cell Biol 13:8–9. CrossRef Medline

Burré J, Sharma M, Tsetsenis T, Buchman V, Etherton MR, Südhof TC (2010) Alpha-synuclein promotes SNARE-complex assembly in vivo and in vitro. Science 329:1663–1667. CrossRef Medline

Cabin DE, Shimazu K, Murphy D, Cole NB, Gottschalk W, McIlwain KL, Orrison B, Chen A, Ellis CE, Paylor R, Lu B, Nussbaum RL (2002) Synaptic vesicle depletion correlates with attenuated synaptic responses to prolonged repetitive stimulation in mice lacking α-synuclein. J Neurosci 22:8797–8807. Medline

Chandra S, Gallardo G, Fernández-Chacón R, Schlüter OM, Südhof TC (2005) Alpha-synuclein cooperates with CSPalpha in preventing neurodegeneration. Cell 123:383–396. CrossRef Medline

Chung CY, Koprich JB, Siddiqi H, Isacson O (2009) Dynamic changes in presynaptic and axonal transport proteins combined with striatal neuroinflammation precede dopaminergic neuronal loss in a rat model of AAV α-synucleinopathy. J Neurosci 29:3365–3373. CrossRef Medline

Chung YH, Joo KM, Kim MJ, Cha CI (2003) Immunohistochemical study on the distribution of alpha-synuclein in the central nervous system of transgenic mice expressing a human Cu/Zn superoxide dismutase mutation. Neurosci Lett 342:151–154. CrossRef Medline

Darios F, Ruipérez V, López I, Villanueva J, Gutierrez LM, Davletov B (2010) Alpha-synuclein sequesters arachidonic acid to modulate SNARE-mediated exocytosis. EMBO Rep 11:528–533. CrossRef Medline

Franklin KBJ, Paxinos G (2008) The mouse brain in stereotaxic coordinates, Ed 3. New York: Academic.

Fujiwara H, Hasegawa M, Dohmae N, Kawashima A, Masliah E, Goldberg MS, Shen J, Takio K, Iwatsubo T (2002) alpha-Synuclein is phosphorylated in synucleinopathy lesions. Nat Cell Biol 4:160–164. Medline

Furuya T, Hayakawa H, Yamada M, Yoshimi K, Hisahara S, Miura M, Mizuno Y, Mochizuki H (2004) Caspase-11 mediates inflammatory dopaminergic cell death in the 1-methyl-4-phenyl-1,2,3,6-tetrahydropyridine mouse model of Parkinson's disease. J Neurosci 24:1865–1872. CrossRef Medline